Simultaneous Targeting of NQO1 and SOD1 Eradicates Breast Cancer Stem Cells via Mitochondrial Futile Redox Cycling

Ming Luo[1,2], Na Shen[2,3], Li Shang[2], Zeng Fang[1,2], Ying Xin[2], Yuxi Ma[2,4], Min Du[1], Yuan Yuan[1], Chenchen Hu[1], Yun Tang[1], Jing Huang[1], Wei Wei[1], Myung Ryul Lee[5], Paul J. Hergenrother[5], and Max S. Wicha[2]

ABSTRACT

Triple-negative breast cancer (TNBC) contains the highest proportion of cancer stem-like cells (CSC), which display intrinsic resistance to currently available cancer therapies. This therapeutic resistance is partially mediated by an antioxidant defense coordinated by the transcription factor NRF2 and its downstream targets that include NAD(P)H quinone oxidoreductase 1 (NQO1). In this study, we identified the antioxidant enzymes NQO1 and superoxide dismutase 1 (SOD1) as therapeutic vulnerabilities of $ALDH^+$ epithelial-like CSCs and $CD24^{-/lo}CD44^{+/hi}$ mesenchymal-like CSCs in TNBC. Effective targeting of these CSC states was achieved by using isobutyl-deoxynyboquinone (IB-DNQ), a potent and specific NQO1-bioactivatable futile redox cycling molecule, which generated large amounts of reactive oxygen species including superoxide and hydrogen peroxide. Furthermore, the CSC killing effect was specifically enhanced by genetic or pharmacologic inhibition of SOD1, a copper-containing superoxide dismutase highly expressed in TNBC. Mechanistically, a significant portion of NQO1 resides in the mitochondrial intermembrane space, catalyzing futile redox cycling from IB-DNQ to generate high levels of mitochondrial superoxide, and SOD1 inhibition markedly potentiated this effect, resulting in mitochondrial oxidative injury, cytochrome c release, and activation of the caspase-3–mediated apoptotic pathway. Treatment with IB-DNQ alone or together with SOD1 inhibition effectively suppressed tumor growth, metastasis, and tumor-initiating potential in xenograft models of TNBC expressing different levels of NQO1. This futile oxidant-generating strategy, which targets CSCs across the epithelial–mesenchymal continuum, could be a promising therapeutic approach for treating patients with TNBC.

Significance: Combining NQO1-bioactivatable futile oxidant generators with SOD1 inhibition eliminates breast cancer stem cells, providing a therapeutic strategy that may have wide applicability, as NQO1 and SOD1 are overexpressed in several cancers.

Introduction

Triple-negative breast cancer (TNBC) is a very aggressive breast cancer subtype with the least favorable prognosis and few treatment options (1, 2). It is also characterized as containing a high proportion of cancer stem-like cells (CSC; refs. 3–5) that contribute to treatment resistance and tumor recurrence (6–9). Many conventional therapies used to treat TNBC such as chemotherapy and radiation actually increase the proportion of CSCs in the residual tumors (10–13), although other studies have suggested that a reversible drug-tolerant persister cell state also mediates chemotherapy resistance (14–16). This highlights the importance of developing strategies to effectively target CSCs and drug-tolerant persister cells in TNBC to improve clinical outcome. CSCs in solid tumors were initially identified in breast cancer by virtue of $CD24^{-/lo}CD44^{+/hi}$ marker expression (17), and subsequent studies have demonstrated that elevated aldehyde dehydrogenase (ALDH) activity also defines a highly tumorigenic cell population in a number of malignancies including breast cancer (18), colon cancer (19, 20), prostate cancer (21), and lung adenocarcinoma (22). More recently, we have demonstrated the phenotypic heterogeneity of these CSC populations, with $CD24^{-/lo}CD44^{+/hi}$ cells representing more mesenchymal/quiescent states and $ALDH^+$ cells representing more epithelial/proliferative CSC states (23). In fact, there is substantial evidence suggesting that rather than representing a fixed, discrete cell population, CSCs represent a highly plastic tumor cell population across the epithelial–mesenchymal transition (EMT)–mesenchymal–epithelial transition (MET) spectrum (24–27). This plasticity facilitates rapid development of epigenetic resistance to targeted therapies and promotes tumor progression and metastasis (26, 28–30). Most attempts to develop CSC-targeted therapies have focused on the targeting of CSC self-renewal pathways such as hedgehog, Notch, and Wnt (31, 32). Although these approaches have shown modest efficacy, their use is limited by CSC heterogeneity and plasticity (27, 33, 34).

An alternative approach for targeting CSCs is to exploit their metabolic vulnerabilities. Despite their regulation by multiple

[1]Department of Breast and Thyroid Surgery, Peking University Shenzhen Hospital, Shenzhen, China. [2]Division of Hematology and Oncology, Department of Internal Medicine, University of Michigan, Ann Arbor, Michigan. [3]Department of Breast and Thyroid Surgery, Union Hospital, Tonji Medical College, Huazhong University of Science and Technology, Wuhan, China. [4]Cancer Center, Union Hospital, Tonji Medical College, Huazhong University of Science and Technology, Wuhan, China. [5]Department of Chemistry, Cancer Center at Illinois, and Carl R. Woese Institute for Genomic Biology, University of Illinois, Urbana, Illinois.

M. Luo and N. Shen contributed equally to this article.

Corresponding Authors: Max S. Wicha, University of Michigan, 2800 Plymouth Road, NCRC 26-335S, Ann Arbor, MI 48109. E-mail: mwicha@med.umich.edu; and Ming Luo, Peking University Shenzhen Hospital, Shenzhen 518036, China. E-mail: luoming@pkuszh.com

Cancer Res 2024;84:4264–82

doi: 10.1158/0008-5472.CAN-24-0800

signal transduction pathways and networks, CSCs maintain metabolic dependencies that are characteristic of their EMT/MET states (35–37). We have shown that redox state of the tumor microenvironment regulates CSC epithelial/mesenchymal (E/M) state dynamics. The generation of oxidant stress facilitates the transition of EMT-like ($CD24^{-/lo}CD44^{+/hi}$) CSCs, which are largely quiescent and dependent on glycolysis, to a more proliferative epithelial cell state characterized by ALDH expression, which is highly dependent on mitochondrial oxidative phosphorylation (37). These $ALDH^+$ CSCs rely on an antioxidant shield coordinated by NRF2 and its downstream targets including NAD(P)H quinone oxidoreductase 1 (NQO1) to survive oxidative stress (37).

NQO1, a cytosolic enzyme involved in NRF2-regulated antioxidant defenses, has emerged as an attractive target for prooxidant–based antitumor strategies (38–40). As a flavin adenine dinucleotide (FAD)-dependent two-electron reductase, NQO1 is overexpressed in many solid tumors including breast cancer (41), colorectal cancer (42), lung cancer (43), gastric adenocarcinoma (44), hepatocellular carcinoma (45), and cervical cancer (46), and high NQO1 expression is associated with poor patient outcomes (46–49), suggesting an important role of NQO1 in promoting cancer progression.

Although NQO1 plays a cytoprotective role in cancer by detoxifying a variety of reactive oxygen species (ROS)–producing quinone toxins, a class of quinone-containing molecules, i.e., β-lapachone (β-Lap) and deoxynyboquinone (DNQ), are subject to NQO1-catalyzed two-electron reduction into unstable hydroquinone-containing molecules, which react with oxygen via two one-electron oxidation steps back to the original quinones, generating large amounts of ROS via the futile redox cycle (50, 51). These NQO1-bioactivatable futile redox cycling compounds (NBRCC) have the potential to turn this normally cytoprotective enzyme into a therapeutic vulnerability for cancer cells that overexpress NQO1 and underexpress catalase (CAT; ref. 40), an enzyme metabolizing hydrogen peroxide.

Despite the role of NBRCCs (i.e., β-Lap) in targeting tumor cells expressing high levels of NQO1 (40, 52–55), the potential of NBRCCs in targeting CSCs remains unstudied. Interestingly, a large array of NRF2-regulated antioxidant genes, including *NQO1*, are markedly elevated in CSCs, especially $ALDH^+$ E-CSCs isolated from patient-derived xenograft models of TNBC (37). This increased NQO1 expression in breast CSCs (BCSC) may serve as a metabolic vulnerability, rendering them susceptible to the ROS generated by NBRCCs. Using a derivative of DNQ, called isobutyl-deoxynyboquinone (IB-DNQ) that exhibited promising efficacy against feline oral squamous cell carcinoma (56), we show here that IB-DNQ is much more potent and specific than β-Lap in killing NQO1-overexpressing TNBC cells with particular efficacy in targeting CSCs. We demonstrate that IB-DNQ–elicited cell death is associated with highly elevated mitochondrial superoxide (MitoROS), which is generated from a portion of NQO1 residing in the mitochondrial intermembrane space (IMS). Furthermore, genetic or pharmacological inhibition of superoxide dismutase 1 (SOD1), but not SOD2 or CAT, synergizes with IB-DNQ to generate MitoROS and abrogate CSCs across the EMT–MET state continuum. By exploiting NQO1 and SOD1 as therapeutic vulnerabilities of CSCs, we demonstrate the use of this oxidant-generating strategy using IB-DNQ alone or together with SOD1 inhibition to suppress tumor growth, metastasis, and tumor-initiating potential in xenograft models of TNBC expressing different levels of NQO1.

Materials and Methods

Cell lines and culture

SUM149 and SUM159 cells were cultured in Ham F12 (Invitrogen) supplemented with 5% FBS (Thermo Fisher Scientific), 5 μg/mL insulin and 1 μg/mL hydrocortisone (both from Sigma-Aldrich), and 10 μg/mL gentamycin and 1% antibiotic–antimycotic (both from Invitrogen). BT20, MDA-MB-231, MDA-MB-468, MDA-MB-157, and MDA-MB-453 were cultured in DMEM–high glucose (Gibco) supplemented with 10% FBS and 1× antibiotic–antimycotic. Vari068, HCC38, HCC70, HCC1937, and ZR-75-1 were maintained in RPMI1640 medium (Thermo Fisher Scientific) supplemented with 10% FBS and 1× antibiotic–antimycotic. MCF7 cells were cultured in Eagle's minimum essential medium (ATCC 30-2003) supplemented with 10% FBS, 10 μg/mL human insulin, and 1× antibiotic–antimycotic. MCF10A is cultured in DMEM/F12 media (50:50, Thermo Fisher Scientific) supplemented with 5% horse serum, 1× HEPES, 20 ng/mL EGF, 0.5 mg/mL hydrocortisone, 100 ng/mL cholera toxin, 10 μg/mL insulin, and 1× antibiotic–antimycotic. Hs578t cells were cultured in DMEM (Gibco) supplemented with 10% FBS, 5 μg/mL insulin, and 1× antibiotic–antimycotic. All the cell lines are cultured at 37°C under 5% CO_2 in a humidified chamber and are *Mycoplasma* free.

MTT and CCK8 assays

For MTT assays, breast cancer cells were seeded at a density of 1,000 to 2,000 cells per well in 96-well microplates overnight and cultured with or without IB-DNQ or β-Lap at various doses alone or with ATN224 (5 μmol/L) or dicumoral (10 μmol/L) for 24 hours. After treatment with drugs, MTT solution was added to each well, and these were incubated for 3 hours. After removing the supernatant, the cells in each well were solubilized by adding 150 μL of DMSO, and optical density (OD) absorbance at 590 nm was measured with a microplate reader (Bio-Rad). Alternatively, cell viability was analyzed using Cell Counting Kit-8 (CCK8, Beyotime Biotechnology) according to the manufacturer's instructions. For CCK8 assay, the cells were seeded at a density of 1,000 to 2,000 cells per well in 96-well microplates overnight. Cells were then treated with various concentrations of IB-DNQ for 24 hours and subsequently 10 μL of CCK8 reagent was added to each well, and then this was cultured for 2 hours. OD absorbance at 450 nm was analyzed with a microplate reader using wells without cells as blanks. Relative cell survival versus control cells was plotted.

DNA constructs and lentiviral infection

TRIPZ and SMARTvector doxycycline (Dox)-inducible lentiviral short hairpin RNA (shRNA) clones against human NQO1, SOD1, SOD2, and CAT were obtained from Horizon Discovery with the following clone #: V2THS_235287 (shNQO1, TRIPZ), V3IHSHER_10771835 (shNQO1-1, SMARTvector), V3IHSHER_7177739 (shNQO1-2, SMARTvector), V3IHSHER_8909942 (shNQO1-3, SMARTvector), V3THS_369718 (shSOD1, TRIPZ), V3IHSHER_9961124 (shSOD1-1, SMARTvector), V3IHSHER_9099989 (shSOD1-2, SMARTvector), V3THS_307804 (shSOD2, TRIPZ), and V2THS_150247 (shCAT, TRIPZ). Lentiviruses expressing human shNQO1, shSOD1, shSOD2, shCAT, or a scrambled sequence (SCR) were packaged at the Vector Core at the University of Michigan. Vari068, HCC70, SUM149, and SUM159 TNBC cells were infected with lentiviruses in the presence of

polybrene (8 μg/mL, Millipore), and the medium containing lentiviruses was replaced with fresh medium after 20 hours of lentiviral infection. Puromycin (Invitrogen) selection was performed at a final concentration of 0.5 to 2.5 μg/ mL for 2 weeks to establish Dox-inducible shNQO1, shSOD1, shSOD2, shCAT, or SCR cell lines.

Cell labeling and flow cytometry

To determine the effect of drug treatment on M- and E-BCSCs in basal breast cancer cell lines, SUM149, SUM159, or Vari068 after various treatments were digested by 0.25% trypsin-EDTA, resuspended in Hank's buffer (HF) (Hank's Balanced Salt Solution plus 2% FBS) at 2×10^5 cells/100 μL and incubated with antibodies against human CD24 (PE-Cy7 conjugated, 1:100, from BD Biosciences for SUM149 or 1:50, from BioLegend for SUM159 and Vari068) and CD44 (APC conjugated, 1:200, from BD Biosciences) in a cold room for 30 minutes. Content of $ALDH^+$ E-BCSCs was determined by ALDEFLUOR assay (STEMCELL Technologies) per the manufacturer's instructions. After labeling, cells were washed two times, resuspended in ALDEFLUOR assay buffer containing 1 μg/mL of 4′,6-diamidino-2-phenylindole (DAPI; Sigma-Aldrich) to discriminate live from dead cells. To obtain tumor cells from tumor xenografts, tumors of SUM149 xenografts grown in SCID mice were digested into single cells by collagenase for an hour and briefly shaken every 15 minutes. Cells debris was removed by filtration through a 40-μm cell strainer (BD Biosciences) to obtain single-cell suspensions. Red blood cells were removed with 0.8% ammonium chloride solution. The dissociated single tumor cells were resuspended in HF (1× Hank's Balanced Salt Solution supplied with 2% FBS) buffer and incubated first with antibody against mouse H2Kd (PE conjugated, 1:100, BD Biosciences) in a cold room for 30 minutes. Tumor cells were obtained by gating out mouse $H2Kd^+$ cells. Flow analysis or sorting was performed using a MoFlow XDP or Astrios Cell Sorter (Beckman Coulter) at the Flow Cytometry Core facility at the University of Michigan.

Analysis of cellular ROS/superoxide and MitoROS

To measure cellular ROS and mitochondrial superoxide levels, cells were stained with CellROX Orange or MitoSOX Red (all from Thermo Fisher Scientific), which generates florescent signals when oxidized by cellular ROS or mitochondrial superoxide in the cells. Cells were incubated with prewarmed CellROX or MitoSOX Red (diluted in PBS to a final concentration of 2.5 μmol/L) staining solution for 30 minutes at 37°C. All subsequent steps were performed in the dark. Cells were washed in PBS, harvested, and then analyzed by flow cytometry. Cellular superoxide levels were labeled with the Cellular Superoxide Detection Assay Kit (ab139477, Abcam) following manufacturer's instructions and analyzed by flow cytometry. Flow data analysis was performed using FlowJo software.

Oxygen consumption and ATP assay

Extracellular oxygen consumption from SUM159 breast cancer cells treated with IB-DNQ or mock (DMSO) was measured using a commercially available assay kit following manufacturer's instructions (Abcam, ab197243). Cellular ATP levels in SUM159 breast cancer cells treated with IB-DNQ or mock (DMSO) were examined with the ATP assay kit from Beyotime Biotechnology (S0026) following the manufacturer's instructions. Fluorescence (for oxygen consumption assay) or luminescence (for ATP assay) intensity was measured using the BioTek Synergy H1 microplate reader.

Apoptosis and mitochondrial membrane potential assay

Apoptotic cells in cultured Vari068 or SUM149 breast cancer cells after IB-DNQ, ATN224 alone, or combined treatment were determined by labeling with APC–Annexin V (BD Biosciences, 1:50) and DAPI and subjected to flow cytometry to detect Annexin V staining. To determine mitochondrial membrane potential, Vari068 or SUM149 breast cancer cells after IB-DNQ, ATN224 alone, or combined treatment were labeled with TMRM perchlorate labeled with PE (PE-TMRM; Invitrogen, 20 nmol/L) for 30 minutes at 37°C. Cells were then washed and incubated with DAPI (Sigma-Aldrich) for 10 minutes at room temperature. After washing with PBS, cells were subjected to analysis by flow cytometry, using 488 nm laser for excitation and a 570 nm emission filter for detection.

TUNEL assay and immunofluorescent staining

Vari068 or SUM149 breast cancer cells were seeded at a density of 2,000 to 5,000 cells per slide for 1 day and then treated with vehicle (DMSO), IB-DNQ, ATN224 alone or in combination with IB-DNQ and ATN224 for 20 hours. Cells were fixed with 4% paraformaldehyde in PBS for 30 minutes at room temperature, rinsed with PBS, and then incubated in permeabilization buffer (0.5% Triton X-100 diluted in PBS) for 15 minutes on ice. Cells were rinsed two times with PBS and incubated with 50 μL of terminal deoxynucleotidyl transferase–mediated dUTP nick end labeling (TUNEL) reaction mixture per sample. For the negative control, 50 μL of Label Solution was used. Cells were incubated with TUNEL reaction mixture for 60 minutes at 37°C in a humidified atmosphere in the dark and rinsed three times with PBS. For immunostaining of ALDH1A3, TUNEL-labeled cells were further incubated with antibodies against ALDH1A3 (Invitrogen, Cat. # PA5-29188, 1:100) in PBS containing 0.5% Triton X-100% and 5% BSA overnight at 4°C, washed with PBS three times, and then incubated with FITC-conjugated goat antirabbit IgG (Jackson ImmunoResearch, 1:200) for 1 hour at room temperature and washed with PBS three times. All cell samples were mounted with VECTASHIELD mounting medium with DAPI (Vector Laboratories). Slides were examined under a BX41 microscope (Olympus) using UplanF1 20× to 40×/0.5 objective lenses. Images were captured with a DP70 camera with DP controller version 1.2.1.108 (Olympus).

Confocal microscopy

SUM159 breast cancer cells seeded at a density of 2,000 to 5,000 cells per slide were fixed with 4% paraformaldehyde, permeabilized with 0.5% Triton X-100 (diluted in PBS) on ice, and blocked in 5% BSA buffer (diluted in PBS) for 1 hour. Cells were then incubated with primary antibodies against NQO1 (cat. #62262 S, Cell Signaling Technology, 1:100) and cytochrome c (Cyto c; cat. #12963 S, Cell Signaling Technology, 1:100) in PBS containing 0.5% Triton X-100 and 5% BSA overnight at 4°C. Subsequently, cells were washed three times with PBS, and incubated with rhodamine-conjugated goat anti-mouse IgG (Jackson ImmunoResearch, 1:200) and FITC-conjugated goat anti-rabbit IgG (Jackson ImmunoResearch, 1:200) at room temperature for 1 hour. Nuclei were stained with DAPI in the dark for 5 minutes at room temperature and mounted with VECTASHIELD mounting medium (Vector Laboratories). Cells were imaged using a confocal microscope (Zeiss LSM 700). Colocalization of NQO1 and Cyto c was analyzed by NIS-Elements software.

Cell fractionation assay

To determine NQO1 and SOD1 expression levels in the mitochondria and cytosol fractions, breast cancer cells treated with

vehicle (DMSO) or IB-DNQ, ATN224, or IB-DNQ plus ATN224 were harvested by a cell scraper in ice-cold PBS, and cells were centrifuged for 5 minutes at 600*g*. Freshly prepared 1× Extraction Buffer A (1 mL) was added per 1×10^7 cells per sample, and cells were incubated on ice for 10 to 15 minutes. Cells were then homogenized on ice using a Dounce homogenizer for 10 to 30 strokes. Cell homogenates were subject to centrifugation at 600*g* for 10 minutes at 2°C to 8°C, and supernatants from different cell samples were carefully transferred to a fresh tube and centrifuged at 11,000*g* for 10 minutes at 2°C to 8°C. The resulting supernatant (cytosol) fractions were carefully removed, and the pellet fractions (mitochondria) were each resuspended in 150 to 200 μL of CelLytic M cell lysis reagent with a protease inhibitor cocktail [1:100 (v/v), Sigma-Aldrich] for further testing.

Transmission electron microscopy

Cells were fixed at 4°C overnight in 3% glutaraldehyde, 3.0% paraformaldehyde in 0.1 mol/L sodium cacodylate buffer, pH 7.2, and were processed by the electron microscopy facility at the University of Michigan. Samples in 70-nm sections on copper grids were examined using the JEOL JEM-1400Plus transmission electron microscope equipped with an XR401 sCMOS camera.

Western blotting

Total cell protein was extracted with RIPA buffer (10 mmol/L Tris-Cl, 100 mmol/L NaCl, 2 mmol/L EDTA, 20 mmol/L NaF, 5 mmol/L Na_3VO_4, 0.5% sodium deoxycholate, 0.1% SDS, and 1% Triton X-100) supplemented with protease and phosphatase inhibitor cocktail (Thermo Fisher Scientific). Cell lysates (20 μg per lane) were lead to and subjected to SDS-PAGE with Bolt 4% to 12% Bis-Tris Plus Gel, blotted onto the polyvinylidene difluoride membrane (Thermo Fisher Scientific), and then blocked with 2% BSA in TBS buffer with 0.1% Tween 20 (TBST) buffer for 1 hour before incubation with primary antibodies as listed in the key resource table (see Supplementary Material). The membrane was rinsed three times in TBST for 5 minutes each time and incubated with horseradish peroxidase–conjugated rabbit or mouse secondary antibodies (Cell Signaling Technology). Protein bands were visualized using WesternBright Sirius chemiluminescent detection kit (Advansta).

Tumorsphere formation assay

For tumorsphere culture of breast cancer cell lines transduced with shNQO1, shSOD1, shSOD2, shCAT, or SCR, 20 live ($DAPI^-$) breast cancer cells were sorted into each well of the 96-well ultralow attachment plate (Corning) containing 150 μL of completed human MammoCult medium (StemCell Technologies) supplemented with 4 μg/mL heparin, 1 μg/mL hydrocortisone, 1% antibiotic–antimycotic, and 20 μg/mL gentamycin (all from Invitrogen) and cultured for 7 to 10 days in the presence of Dox (0.5 μg/mL) together with or without IB-DNQ. Tumorspheres with diameter more than 40 μmol/L were counted under an optical microscope with 10× optical lens (EVOS all-in-one digital inverted microscope) and plotted for mean sphere formation per 100 cells. Tumorspheres of parental SUM149, SUM159, or Vari068 breast cancer cells under various drug treatment regimens were cultivated at the condition of 20 cells/well in completed human MammoCult medium for 7 to 10 days. Tumorspheres settled in these conditions were counted under an optical microscope with 10× optical lens using the EVOS all-in-one digital inverted microscope.

Animal studies and drug treatment

Seven-week-old female SCID mice were purchased from Charles River Laboratories and housed in Association for Assessment and Accreditation of Laboratory Animal Care International–accredited specific pathogen-free rodent facilities at the University of Michigan. Tumor growth was determined by injecting primary breast cancer cells (Vari068: 1×10^6 cells per site; SUM49: 0.5×10^6 cells per site) with 30% Matrigel (BD Biosciences) into the fourth mammary fat pad (MFP) of 7-week-old female SCID mice, with six to eight mice per cohort. Mouse treatments were started when the tumors reached 3 to 5 mm in diameter using vehicle [20% hydroxypropyl-β-cyclodextrin (HPβCD), i.v.], IB-DNQ (10 mg/kg), ATN224 (10 mg/kg), or combined treatment (i.v., every 2 days). Tumor size was measured one time a week with a caliper and calculated as tumor volume = length × $\text{width}^2/2$. Animals were euthanized at the end of treatments. Vari068 tumor xenografts and lung tissue sections were monitored by hematoxylin and eosin staining and IHC. For limiting-dilution secondary transplantation, SUM149 xenograft tumors were dissociated into single cells, and tumor cells of human origin were obtained by gating out mouse $H2Kd^+$ cells. $H2Kd^-$ primary tumor cells sorted by using flow cytometry were prepared in 30% Matrigel (BD Biosciences) with two or three different dilutions and injected bilaterally into the fourth MFP of 7-week-old female SCID mice, with three to four mice per dilution. Tumor appearance was monitored for 3 months, and the frequency of tumor-initiating cells was calculated using the ELDA software (Walter and Eliza Hall Institute of Medical Research).

To study the impact of SOD1 knockdown (KD) on IB-DNQ sensitivity *in vivo*, SUM149 cells harboring shSOD1 and SCR were injected into the fourth MFP of 7-week-old female SCID mice (1×10^6 per site). On the following day, mice (both shSOD1 and SCR) were randomly divided into vehicle or IB-DNQ treatment cohort ($n = 6$). Water containing Dox (200 μg/mL, Sigma-Aldrich) was administrated to each mouse cohort via bottled water supplied at day 1 after tumor cell implantation. IB-DNQ (10 mg/kg) or vehicle (20% HPβCD) treatments were started when the tumors reached 3 to 5 mm in diameter by tail vein injection. IB-DNQ or vehicle was given intravenously, every 2 days. Tumor size was measured once time a week with a caliper and calculated as tumor volume = length × $\text{width}^2/2$. All mouse experiments were performed in accordance with protocols approved by the Institutional Animal Care and Use Committee at the University of Michigan.

Kaplan–Meier analysis

Analysis of NQO1, SOD1, SOD2, and CAT antioxidant genes in a database of 4,929 patients with breast cancer (including all molecular subtypes) was performed using the Kaplan–Meier plotter (http://kmplot.com/analysis/index.php?p=service&default=true). Selected genes with correlation to patient survival were further analyzed using restricted analysis to different molecular subtypes of breast cancer.

Statistical analysis

All *in vitro* assays were independently performed at least three times unless otherwise specified. Statistical differences between two groups were calculated using two-tailed Student *t* test. Statistical differences between three or more groups were calculated using one-way ANOVA with Bonferroni correction. Two-way ANOVA was used to analyze the extracellular oxygen consumption or tumor growth of TNBC cells with different treatments at multiple intervals.

All analyses were conducted using GraphPad Prism (version 8.0). Unless otherwise indicated, data are presented as the mean ± SEM, and a two-tailed value of *, $P < 0.05$; **, $P < 0.01$; ***, $P < 0.001$ and ****, $P < 0.0001$ was considered statistically significant.

Data availability

Data supporting the findings of this study are available within the article and its Supplementary Material. Raw data are available from the corresponding authors upon request.

Results

NQO1 and SOD1 are highly expressed in TNBC and are associated with poor patient survival

To identify potential biomarkers predicting treatment responses to IB-DNQ, we examined the expression of NQO1 in a large panel of patients with TNBC using a tumor tissue array versus two normal breast tissues (**Fig. 1A**), which unveiled that NQO1 is overexpressed in more than 90% of TNBC versus normal breast tissues. NQO1 overexpression in TNBC provides a therapeutic vulnerability exploitable by NQO1-bioactivatable futile redox cycling from NBRCCs (i.e., IB-DNQ), which produces large amounts of superoxide (O_2^-) and downstream ROS (**Fig. 1B**).

Because a high NQO1/CAT ratio in non–small cell lung cancer promotes therapeutic efficacy of β-Lap (40), we next examined the expression pattern of NQO1 and the related antioxidant enzymes including CAT, SOD1, and SOD2 across 13 TNBC cell lines versus a nontumorigenic mammary epithelial cell line, MCF10A. NQO1 is overexpressed in a large proportion of TNBC cells, with five cell lines (Vari068, MDA-MB-453, HCC38, HCC1937, and Hs578t) expressing high levels of NQO1 ($NQO1^{hi}$), three (MDA-MB-157, SUM159, and HCC70) expressing medium levels ($NQO1^{med}$), and two (HCC1806 and SUM149) expressing low levels of NQO1 ($NQO1^{lo}$) when compared with MCF10A (**Fig. 1C**). In addition, three cell lines (MDA-MB-231, MDA-MB-468, and BT20) displayed no detectable NQO1 ($NQO1^{null}$), presumably due to a *2 mutation (C609 T) that promotes NQO1 degradation (57, 58).

Surprisingly, CAT, a H_2O_2 detoxifying enzyme underexpressed in non–small cell lung cancer but highly expressed in benign tissues (40), is expressed in TNBC cells, and three TNBC lines have significantly elevated CAT expression (**Fig. 1C**). However, SOD1, a cytosolic, copper-containing enzyme, is ubiquitously overexpressed across all 13 TNBC cells, whereas SOD2, a superoxide dismutase localized in the mitochondria, is either unchanged (6/13) or suppressed (7/13) versus MCF10A (**Fig. 1C**). These data support the notion that a SOD2-to-SOD1 switch occurs during breast oncogenesis (59). We also examined the overall expression of ALDH1A1/A3, two established BCSC markers. Vari068, SUM149, HCC38, and HCC1937 express ALDH1A3 but not ALDH1A1, whereas SUM159, a mesenchymal breast cancer cell line, expresses ALDH1A1 but not ALDH1A3 (**Fig. 1C**). The identification of $NQO1^{+}$ TNBC cells expressing ALDH1A1/A3 provides suitable cell models to evaluate the potential of IB-DNQ in targeting $ALDH^{+}$ CSCs.

As NQO1 and SOD1 are overexpressed in TNBC versus the normal mammary epithelial cell, we next determined if the expression of these antioxidant enzymes correlate with disease progression across different breast cancer subtypes. Kaplan–Meier analysis of a publicly available database of 4,929 patients with breast cancer (60) revealed that high NQO1 expression correlates with low recurrence-free survival in the whole breast cancer cohort (**Fig. 1D**), and in the luminal A (Supplementary Fig. S1A), luminal B (Supplementary Fig. S1B), $HER2^{+}$ (Supplementary Fig. S1C), and basal (**Fig. 1E**) breast cancer cohorts, suggesting a universal role of NQO1 in promoting cancer progression. High SOD1 expression also correlates with low recurrence-free survival in the whole (Supplementary Fig. S1D) and basal breast cancer (Supplementary Fig. S1E) cohort. By contrast, CAT (Supplementary Fig. S1F and S1G) or SOD2 (Supplementary Fig. S1H and S1I) expression did not correlate with patient survival in the whole and basal breast cancer cohort. These studies suggest that NQO1 and SOD1, but not CAT or SOD2, may play more significant roles in breast cancer progression.

NQO1 is highly expressed in TNBC CSCs

$ALDH^{+}$ CSCs are endowed with elevated NRF2 antioxidant defenses (37). Double labeling immunofluorescence of TNBC tissues using specific antibodies against NQO1 and ALDH1 revealed that NQO1 is highly expressed in $ALDH1^{+}$ CSCs and bulk tumor cells (**Fig. 1F**). As tumorspheres enrich for CSCs, we compared the expression of NQO1 and its related antioxidant enzymes (NRF2, CAT, SOD1, and SOD2) in TNBC cells cultured as three-dimensional spheroids versus two-dimensional adherent cells. NQO1, NRF2, CAT, SOD1, and SOD2 are all overexpressed in spheroid cells of different TNBC lines (**Fig. 1G**).

To validate if CSCs in different E/M states exhibit elevated NQO1 expression, we used SUM159 to sort $ALDH^{hi}$ CSCs as well as $ALDH^{med}$ and $ALDH^{-}$ bulk breast cancer cells (**Fig. 1H**) and examined NQO1 expression. NQO1 is elevated in $ALDH^{+}$ ($ALDH^{hi}$ and $ALDH^{med}$) cells versus $ALDH^{-}$ bulk breast cancer cells (**Fig. 1I**). Using basal breast cancer cells, SUM149 that harbor CSCs in distinct E/M states, we sorted $ALDH^{+}$ E- and $ALDH^{-}CD24^{-}CD44^{+}$ M-CSCs and $ALDH^{-}CD24^{+}CD44^{-}$ differentiated cells and examined their relative NQO1 expression. Both E- and M-CSCs from SUM149 display elevated NQO1 expression versus differentiated breast cancer cells (**Fig. 1J**). This elevated NQO1 expression in CSCs may render them vulnerable to NQO1-bioactivatable futile redox cycling.

IB-DNQ is more potent and specific than β-Lap in killing TNBC cells in an NQO1-dependent fashion

We compared the potency of IB-DNQ versus β-Lap, a highly studied NBRCC, in killing Vari068 TNBC cells developed from a primary tumor xenograft (37), which highly expresses NQO1 (**Fig. 1C**). IB-DNQ kills Vari068 cells (24 hours treatment) with 50% lethal dose (LD_{50}) of 63 nmol/L, which is 60-fold more potent than β-Lap (LD_{50} at 3.8 μmol/L). Interestingly, cell lethality elicited by IB-DNQ but not β-Lap is fully rescued by dicoumarol (DIC, an NQO1 specific inhibitor; **Fig. 2A–C**). Similar studies were conducted in SUM159 (Supplementary Fig. S2A–S2C) and MDA-MB-157 (Supplementary Fig. S2D and S2E), confirming the high potency and specificity of IB-DNQ versus β-Lap in targeting TNBC cells overexpressing NQO1. We also tested the potency of IB-DNQ versus β-Lap in HCC1806 cells that express low levels of NQO1 when compared with MCF10A. IB-DNQ kills HCC1806 cells with LD_{50} of 405 nmol/L, which is significantly more potent than β-Lap (LD_{50} >5 μmol/L), and cell lethality elicited by IB-DNQ and β-Lap in HCC1806 cells are both rescued by DIC (Supplementary Fig. S2F and S2G).

The MTT assay used to measure cell viability is based on mitochondrial dehydrogenase activity, which may be a direct target of NBRCCs. We made a comparison using CCK8 (which involves most of the dehydrogenase activity in the cell) versus MTT assay on

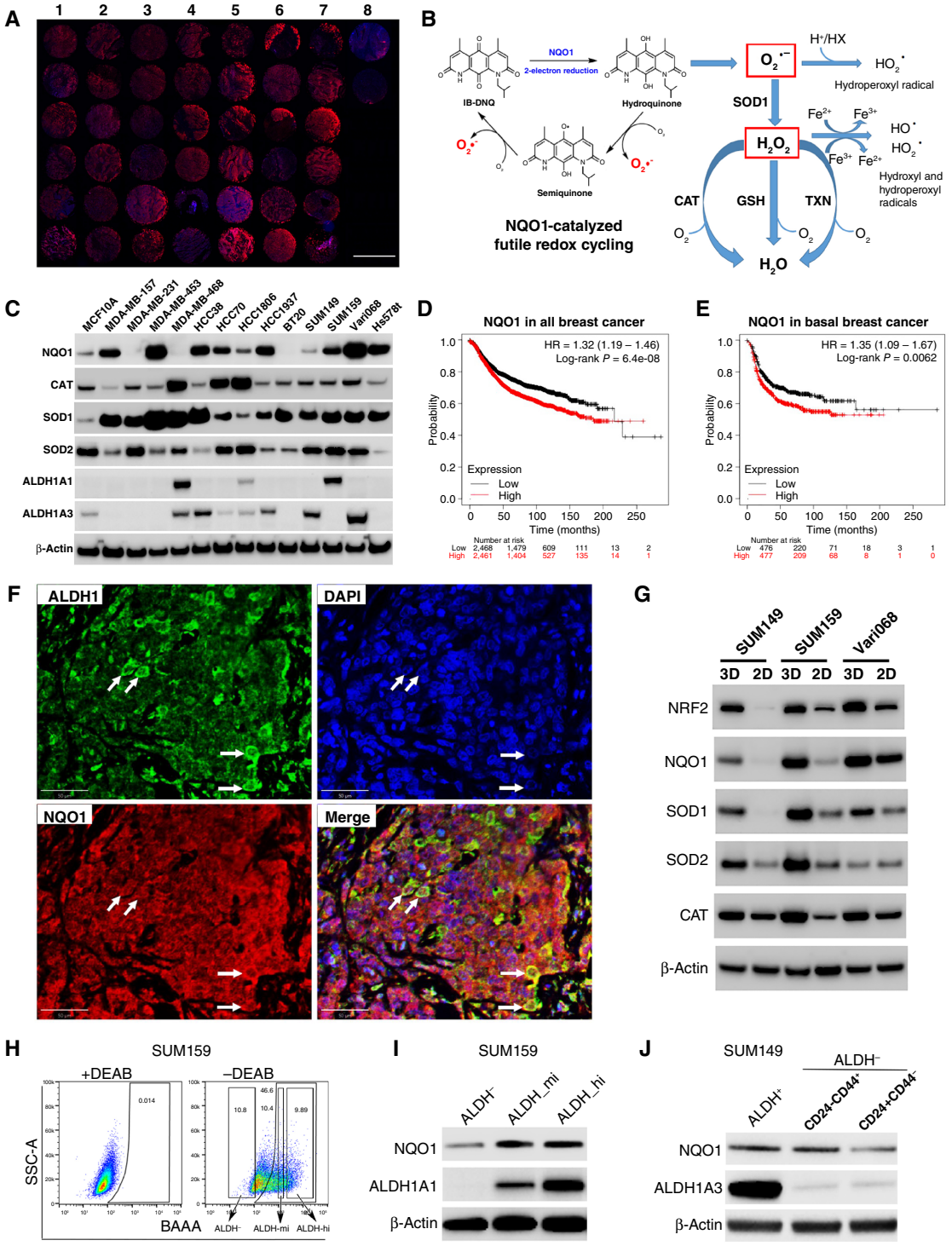

Figure 1.

NQO1 and related antioxidant enzyme expression in TNBC tissues, cell lines, and CSC populations. **A,** Immunofluorescent labeling of NQO1 in a human TNBC tissue array (columns 1 to 7) vs. two normal mammary tissues (column 8). Scale bar, 2 mm. **B,** NQO1-catalyzed futile redox cycle from IB-DNQ. GSH, glutathione; TXN, thioredoxin. **C,** NQO1 and related antioxidant enzyme expression in 13 TNBC cell lines vs. MCF10A. **D** and **E,** NQO1 expression predicts poor recurrence-free survival in a patient cohort containing all breast cancer subtypes (**D**) and basal breast cancer (**E**). **F,** Double labeling of TNBC tissues using specific antibodies against NQO1 and ALDH1. Bar, 50 μm. **G,** NQO1 and its related antioxidant enzyme expression in tumorspheres vs. two-dimensional adherent cells. **H** and **I,** $ALDH^{hi}$, $ALDH^{med}$, and $ALDH^{-}$ bulk tumor cells were sorted based on ALDEFLUOR assay (**H**) and examined by immunoblotting with ALDH1A1 and NQO1 antibodies (**I**). **J,** NQO1 expression in $ALDH^{+}$ and $ALDH^{-}CD24^{-}CD44^{+}$ CSCs vs. bulk tumor cells of SUM149.

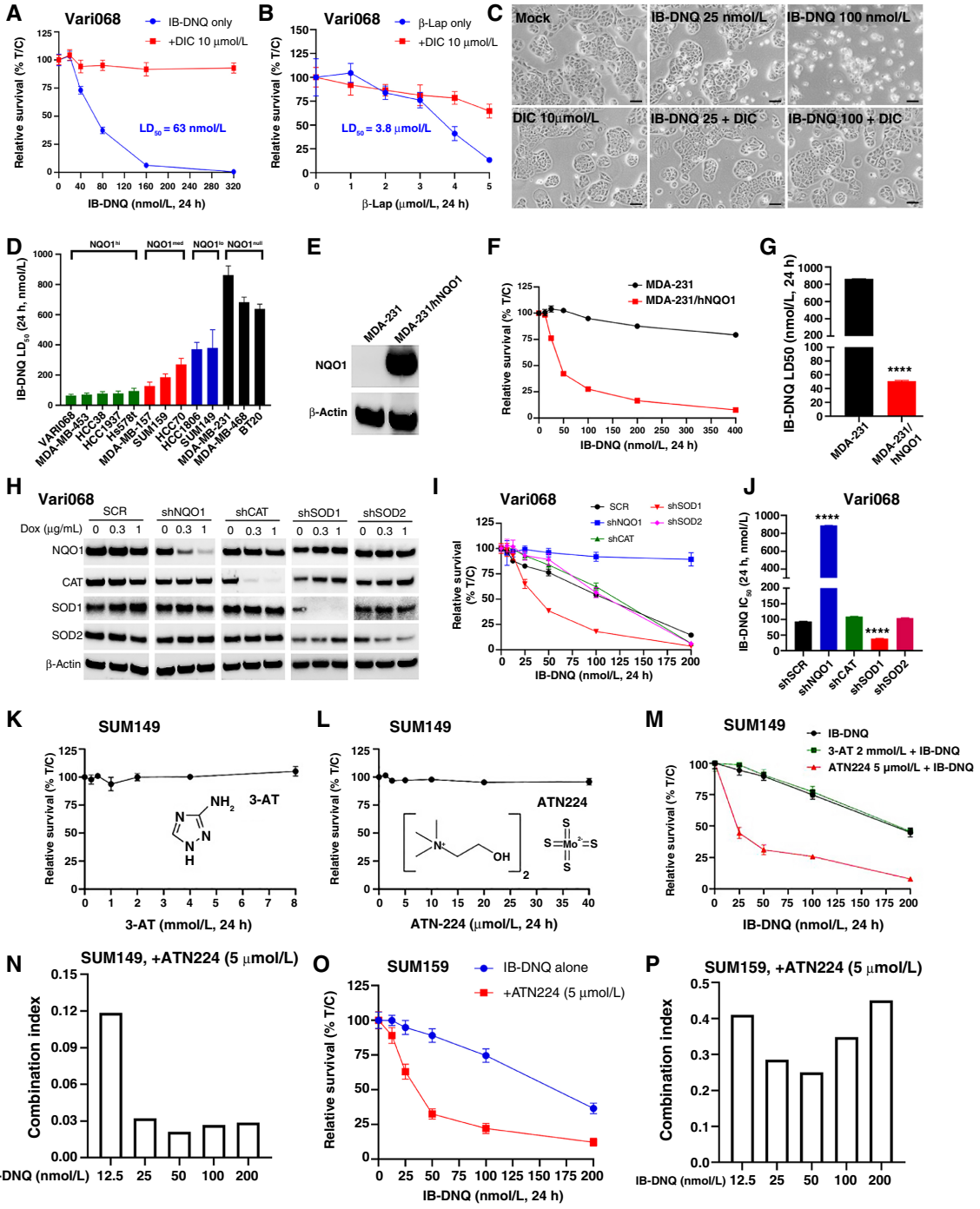

Figure 2.

IB-DNQ is more potent and specific than β-Lap in killing TNBC cells, and genetic or pharmacologic inhibition of SOD1 synergistically enhances IB-DNQ–elicited lethality. **A** and **B,** LD_{50} of IB-DNQ (**A**) vs. β-Lap (**B**) in Vari068 breast cancer cells treated with or without DIC ($n = 6$ wells). **C,** Vari068 cells treated with Mock, DIC (10 μmol/L), IB-DNQ (25 and 100 nmol/L), or IB-DNQ plus DIC (10 μmol/L) for 24 hours and examined by light microscopy. Scale bar, 50 μm. **D,** IB-DNQ LD_{50} in 13 TNBC cells ($n = 2$). **E–G,** NQO1 expression in NQO^- MDA-MB-231 (**E**) renders these cells sensitive to IB-DNQ ($n = 6$ wells; **F**) with LD_{50} <50 nmol/L (**G**). ****, $P < 0.0001$ vs. NQO^- cells ($n = 2$, unpaired Student t test). **H–J,** Dox-inducible KD of NQO1, CAT, SOD1, and SOD2 in Vari068 validated by immunoblotting with respective antibodies (**H**), and relative survival curve ($n = 6$ wells; **I**) and IC_{50} (**J**) of Vari068 cells with KD of NQO1, CAT, SOD1, or SOD2 vs. SCR cells following IB-DNQ treatment. ****, $P < 0.0001$ vs. shSCR ($n = 2$, unpaired Student t test). **K** and **L,** Relative survival of SUM149 treated with 3-AT (**K**) or ATN224 (**L**) at different doses for 24 hours ($n = 6$ wells). **M** and **N,** Relative survival of SUM149 cells treated with IB-DNQ alone or together with ATN224 or 3-AT ($n = 6$ wells; **M**) and combination index of ATN224 (5 μmol/L) with IB-DNQ from 12.5 to 200 nmol/L in SUM149 (**N**). **O** and **P,** Relative survival of SUM159 cells treated with IB-DNQ alone or with ATN224 ($n = 6$ wells; **O**) and combination index of ATN224 with IB-DNQ from 12.5 to 200 nmol/L in SUM159 (**P**).

SUM159 breast cancer cells treated with IB-DNQ. This revealed that IB-DNQ at different doses resulted in the same degree of cytotoxicity determined by MTT versus CCK8 assay (Supplementary Fig. S2H). We further tested the relative survival of SUM159 breast cancer cells treated with IB-DNQ in media containing high (25 mmol/L) versus low (5.5 mmol/L) concentrations of glucose (Supplementary Fig. S2I). This confirms that the sensitivity of TNBC cells to IB-DNQ is independent of glucose concentrations.

We systemically measured the LD_{50} of IB-DNQ in 13 TNBC cell lines and found that the killing potency of IB-DNQ is correlated with NQO1 protein expression levels (**Fig. 2D**). $NQO1^{hi}$ Vari068 and MDA-MB-453 display the highest sensitivity, whereas $NQO1^{null}$ cell lines are resistant to IB-DNQ at doses <500 nmol/L. As $NQO1^{null}$ TNBC cells are resistant to IB-DNQ, we next measured LD_{50} of IB-DNQ in isogenic MDA-MB-231 cells with *NQO1*$^{+}$ (expressing wild-type hNQO1) or *NQO1*$^{-}$ (expressing NQO1 *2 mutation) gene expression. hNQO1 expression (**Fig. 2E**) confers high sensitivity of NQO*1*$^{-}$ cells to IB-DNQ with LD_{50} <50 nmol/L (**Fig. 2F** and **G**).

Genetic or pharmacologic inhibition of SOD1 enhances IB-DNQ–elicited cell lethality

To validate the roles of NQO1, CAT, SOD1, and SOD2 in regulating IB-DNQ–elicited killing of TNBC cells, we used the TRIPZ lentiviral vectors to establish Dox-inducible KD of NQO1, CAT, SOD1 and SOD2 in $NQO1^{hi}$ Vari068, $NQO1^{med}$ HCC70, and $NQO1^{lo}$ SUM149 breast cancer cells. Dox-induced KD of NQO1 in Vari068 (**Fig. 2H–J**) and HCC70 (Supplementary Fig. S2J–S2L) renders these cells resistant to IB-DNQ, whereas the cells expressing an SCR remain sensitive. Surprisingly, Dox-induced KD of CAT in Vari068 and HCC70 had no appreciable effect on IB-DNQ sensitivity. By contrast, Dox-induced KD of SOD1, but not of SOD2, markedly enhanced IB-DNQ sensitivity in Vari068 and HCC70. This increased IB-DNQ sensitivity upon KD of SOD1, but not of CAT, was also observed in $NQO1^{lo}$ SUM149 cells (Supplementary Fig. S2M–S2O). As SOD1 provides major superoxide dismutase activity in breast cancer cells catalyzing H_2O_2 generation from O_2^- (59), our data suggest the ROS effector responsible for IB-DNQ–elicited killing is actually O_2^- rather than H_2O_2, which is thought to mediate β-Lap–induced tumor cell killing by inducing single-stranded DNA breaks and PARP1 hyperactivation, promoting the depletion of NAD^+ and ATP to trigger programmed necrosis (40).

The limited availability of TRIPZ-inducible shRNA clones for NQO1 and SOD1 make it hard to assess the specificity of these shRNAs. To address this issue, we obtained SMARTvector Dox–inducible lentiviral shRNA clones for NQO1 and SOD1 and made additional KD cells against NQO1 and SOD1 in SUM159. After Dox induction, SUM159 breast cancer cells expressing three different NQO1 shRNAs (shNQO1-1/2/3) all had significantly reduced NQO1 expression, with shNQO1-2 and shNQO1-3 displaying the best KD efficiency (Supplementary Fig. S3A, inset). KD of NQO1 with shNQO1-2 or shNQO1-3 rendered SUM159 breast cancer cells more resistant to IB-DNQ (Supplementary Fig. S3A), consistent with the studies using TRIPZ-inducible NQO1 shRNA. Similar studies were done in SUM159 cells using the SMARTvector lentiviral shRNA clones for SOD1 (shSOD1-1/2), which unveiled that Dox-induced KD of SOD1 with shSOD1-2 but not with shSOD1-1 significantly reduced SOD1 expression (Supplementary Fig. S3B, inset), leading to significantly increased IB-DNQ sensitivity.

Having genetically validated NQO1 and SOD1 as two therapeutic targets exploitable by IB-DNQ futile redox cycling, we next asked if pharmacologic inhibition of SOD1 versus CAT enhances the killing efficacy of IB-DNQ in $NQO1^{lo}$ TNBC cells. SUM149 treated with a CAT inhibitor 3-AT (**Fig. 2K**) or SOD1 inhibitor ATN224 alone (**Fig. 2L**) at different doses for 24 hours did not significantly affect tumor cell survival. However, treatment with IB-DNQ together with ATN224 but not 3-AT markedly enhanced IB-DNQ–induced killing of SUM149 breast cancer cells (**Fig. 2M**). Calculation of the combination index of ATN224 at 5 μmol/L with sublethal doses of IB-DNQ from 12.5 to 200 nmol/L confirmed that ATN224 generates strong synergy (combination index <0.15) with IB-DNQ at each dose examined (**Fig. 2N**). Similar synergistic effect of ATN224 with IB-DNQ in killing TNBC cells was observed in $NQO1^{lo}$ HCC1806 (Supplementary Fig. S3C and S3D) and $NQO1^{med}$ SUM159 (**Fig. 2O** and **P**). By contrast, MCF10A treated with IB-DNQ (50–300 nmol/L) plus distinct inhibitors of SOD1, including ATN224 (Supplementary Fig. S3E) or LCS1 (a SOD1 inhibitor without copper-chelating activity; Supplementary Fig. S3F) failed to generate synergistic killing effect. LCS1 (1 μmol/L) with IB-DNQ from 12.5 to 200 nmol/L also synergistically increased IB-DNQ–elicited killing of SUM149 and SUM159 breast cancer cells (Supplementary Fig. S3G–S3I).

IB-DNQ abrogates sphere-forming ability of NQO1-expressing TNBC cells at sublethal concentrations, and SOD1 inhibition potentiates this effect

Using tumorsphere formation at clonal density, an assay that is widely used to assess CSC activity, we observed that IB-DNQ at 25 to 50 nmol/L severely suppressed sphere-forming capacity, exemplified by significantly reduced numbers of spheres and smaller sphere sizes, in Vari068 (**Fig. 3A**; Supplementary Fig. S4A) and SUM159 (**Fig. 3B**; Supplementary Fig. S4B) breast cancer cells that overexpress NQO1. In contrast to significantly inhibited tumorsphere formation, Vari068 (**Fig. 3C**) and SUM159 (**Fig. 3D**) cells grown at two-dimensional adherent culture containing IB-DNQ at 25 to 50 nmol/L for 2 weeks only modestly inhibited tumor cell survival.

We next examined if Dox-induced KD of NQO1, CAT, SOD1, or SOD2 alters IB-DNQ suppression of sphere-forming capacity (**Fig. 3E** and **F**). Vari068 breast cancer cells expressing an SCR exhibit a dose-dependent inhibition of tumorsphere formation in the presence of IB-DNQ (10 or 20 nmol/L) and Dox (0.5 μg/mL), whereas Dox-induced KD of NQO1 renders Vari068 cells resistant to IB-DNQ. Dox-induced KD of CAT does not alter IB-DNQ inhibition of tumorsphere formation, whereas Dox-induced KD of SOD1, but not of SOD2, significantly enhances IB-DNQ suppression of tumorsphere formation. Dox-induced KD of SOD1, but not of NQO1, CAT, or SOD2, slightly but significantly decreases sphere-forming ability of Vari068 cells, suggesting a role of SOD1 in maintaining CSC activity. As observed in Vari068 cells, $NQO1^{lo}$ SUM149 breast cancer cells expressing an SCR exhibited significantly inhibited sphere-forming activity when treated with IB-DNQ, and Dox-induced KD of CAT did not affect SUM149 sphere-forming ability or significantly alter IB-DNQ inhibition of tumorsphere formation (Supplementary Fig. S4C). In contrast to CAT KD, Dox-induced SOD1 KD severely inhibited SUM149 sphere-forming ability, and SOD1 KD together with 20 nmol/L of IB-DNQ completely abrogated SUM149 tumorsphere formation (Supplementary Fig. S4C). SOD2 KD also had an inhibitory effect on SUM149 tumorsphere formation, which failed to enhance IB-DNQ inhibition of sphere-forming ability.

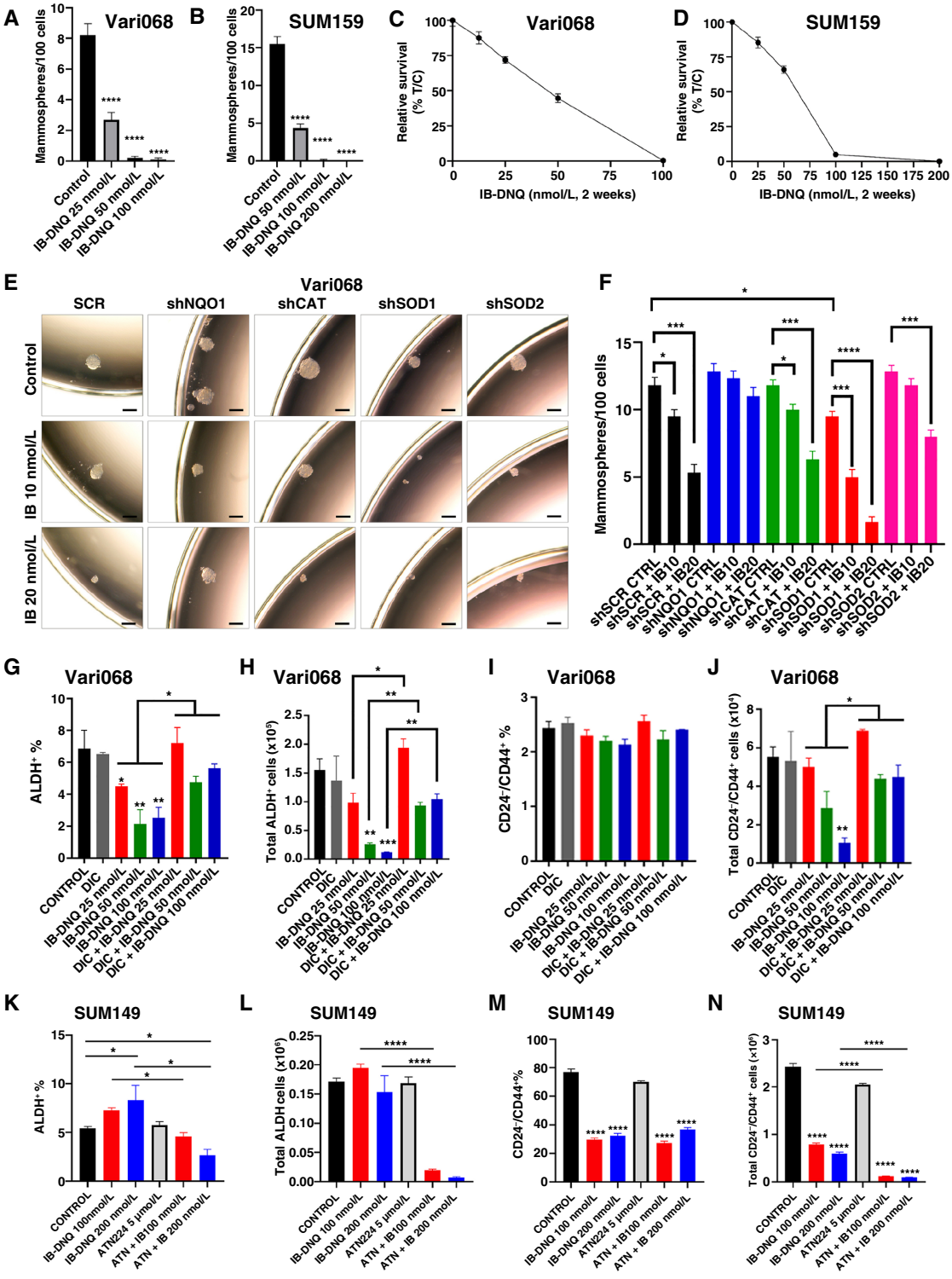

Figure 3.

IB-DNQ treatment preferentially inhibits CSC activity in TNBC cells expressing NQO1. **A–D,** Tumorsphere formation of Vari068 (**A**) and SUM159 (**C**) breast cancer cells in medium containing control (DMSO) or IB-DNQ of various doses, and relative survival of Vari068 (**B**) and SUM159 (**D**) cells grown in adherent culture with IB-DNQ for 14 days, $n = 6$ wells. **E** and **F,** Sphere formation of Vari068 cells subjected to Dox-induced KD of NQO1, CAT, SOD1, or SOD2 and IB-DNQ treatment (**E**) and the impact of KD on IB-DNQ suppression of sphere-forming capacity (**F**). **G–N,** Vari068 (**G–J**) and SUM149 (**K–N**) cells were treated with indicated compounds for 20 hours and examined for the content and absolute number of $ALDH^+$ and $CD24^-CD44^+$ CSCs. *, $P < 0.05$; **, $P < 0.01$; ***, $P < 0.001$; ****, $P < 0.0001$ vs. control or indicated by brackets. $n = 3$, one-way ANOVA for **A**, **C**, **F**, **G–J**, and **K–N**.

We determined if pharmacological inhibition of SOD1 is synergistic with IB-DNQ in suppressing CSC activity. SUM149 breast cancer cells treated with 2.5 μmol/L of ATN224 or 50 nmol/L of IB-DNQ each exhibited significantly inhibited sphere-forming capacity, and cotreatment with ATN224 and IB-DNQ completely blocked tumorsphere formation (Supplementary Fig. S4D). In SUM159 breast cancer cells, an increased concentration of ATN224 is required to inhibit tumorsphere formation, and ATN224 together with IB-DNQ generated a strong synergy, inhibiting sphere-forming capacity (Supplementary Fig. S4E).

NQO1 and SOD1 maintain ALDH$^+$ E-CSCs and CD24$^-$CD4$^+$ M-CSCs, respectively, and SOD1 inhibition augments IB-DNQ redox cycling to abrogate both E- and M-CSCs

IB-DNQ treatment of Vari068 (**Fig. 3G** and **H**) and SUM159 (Supplementary Fig. S5A and S5B) breast cancer cells dose-dependently decreased the percentage and absolute cell number of ALDH$^+$ CSCs, which were rescued by DIC. Despite that IB-DNQ preferentially targets ALDH$^+$ CSCs in TNBC cells overexpressing NQO1, it failed to reduce the proportion of CD24$^-$CD44$^+$ M-CSC-like cells in Vari068 (**Fig. 3I**) and SUM159 (Supplementary Fig. S5C), although the absolute number of M-CSC–like cells in Vari068 (**Fig. 3J**) and SUM159 (Supplementary Fig. S5D) were significantly reduced, which were rescued by DIC. Although Dox-induced KD of NQO1 in Vari068 breast cancer cells renders ALDH$^+$ CSCs (Supplementary Fig. S5E and S5F) and bulk tumor cells (Supplementary Fig. S5G) resistant to IB-DNQ, NQO1 KD in Vari068 significantly reduces the proportion and absolute number of ALDH$^+$ CSCs, supporting a role of NQO1 for the maintenance of ALDH$^+$ CSCs (61).

We next tested if SOD1 inhibition augments IB-DNQ redox cycling to abrogate E- and M-CSCs in TNBC expressing low/modest levels of NQO1. IB-DNQ treatment of SUM149 breast cancer cells had a differential effect on distinct CSC states, with the proportion and absolute number of ALDH$^+$ E-CSCs slightly increased (**Fig. 3K** and **L**), but with the proportion and absolute number of CD24$^-$CD4$^+$ M-CSCs significantly decreased (**Fig. 3M** and **N**). These differential responses of E- and M-CSCs to IB-DNQ reflect the fact that modest levels of ROS produced by IB-DNQ in NQO1^{lo} SUM149 breast cancer cells do not harm but promote ALDH$^+$ E-CSCs. By contrast, ROS^{lo} M-CSCs are sensitive to even modestly increased ROS, which induces their transition to a ROS^{hi} E-CSC state (37). Although IB-DNQ at sublethal doses is not sufficient to decrease ALDH$^+$ E-CSCs in SUM149, cotreatment with IB-DNQ plus ATN224 significantly reduced the percentage and absolute number of E-CSCs (**Fig. 3K** and **L**). ATN224 also potentiates the effect of IB-DNQ in abrogating the absolute number of CD24$^-$CD44$^+$ M-CSCs, despite the percentage of these cells being not further decreased (**Fig. 3M** and **N**).

As a copper-chelating inhibitor of SOD1, ATN224 may have off-target effects by inhibiting other copper-containing proteins, confounding a specific role of SOD1 inhibition in synergizing IB-DNQ redox cycling targeting CSCs. To address this issue, we examined the efficacy of IB-DNQ targeting ALDH$^+$ E- and CD24$^-$CD4$^+$ M-CSCs in SUM149 breast cancer cells expressing Dox-inducible shSOD1 or SCR. In Dox-treated SUM149 breast cancer cells expressing an SCR, distinct CSC states exhibited differential responses to IB-DNQ, with the percentage and absolute number of ALDH$^+$ E-CSCs increased (Supplementary Fig. S5H and S5I), but CD24$^-$CD4$^+$ M-CSCs significantly decreased in a dose-dependent fashion (Supplementary Fig. S5J and S5K). Although IB-DNQ at sublethal doses failed to abrogate but promoted ALDH$^+$ E-CSCs in SUM149 expressing SCR, Dox-induced KD of SOD1 markedly enhanced the efficacy of IB-DNQ to reduce the percentage (Supplementary Fig. S5H) and total number (Supplementary Fig. S5I) of ALDH$^+$ CSCs. Dox-induced SOD1 KD also potentiates the effect of IB-DNQ in abrogating the absolute number of CD24$^-$CD4$^+$ M-CSCs (Supplementary Fig. S5K). Notably, Dox-induced KD of SOD1 in SUM149 selectively decreased the proportion and absolute number of CD24$^-$CD4$^+$ M-CSCs (Supplementary Fig. S5J and S5K) but not ALDH$^+$ E-CSCs (Supplementary Fig. S5H and S5I), suggesting a specific role of SOD1 in maintaining M-CSCs. In SUM159 breast cancer cells, cotreatment with IB-DNQ and ATN224 also synergistically enhances the depletion of ALDH$^+$ CSCs, and this effect was rescued by DIC (Supplementary Fig. S5L and S5M).

IB-DNQ triggers apoptosis of ALDH$^+$ CSCs, and SOD1 inhibition potentiates this effect in TNBC expressing low/modest levels of NQO1

To explore the nature of cell death elicited by IB-DNQ, we first treated NQO1^{hi} Vari068 TNBC cells with sublethal doses of IB-DNQ for 20 hours, which were then labeled with Annexin V and DAPI to assess the cells undergoing early (DAPI$^-$Annexin V$^+$) or late (DAPI$^+$Annexin V$^+$) apoptosis (Supplementary Fig. S6A). IB-DNQ induces both early and late apoptosis of Vari068 breast cancer cells in a dose-dependent manner (**Fig. 4A**). To confirm if IB-DNQ directly induces apoptosis of ALDH$^+$ CSCs, we examined IB-DNQ–treated Vari068 cells by ALDH1A3 and TUNEL (apoptotic marker) dual immunofluorescence. Vari068 breast cancer cells treated with IB-DNQ (0.1 μmol/L) versus vehicle exhibit significantly increased TUNEL$^+$ labeling in ALDH1A3$^+$ CSCs (arrows; **Fig. 4B**), confirming that IB-DNQ at sublethal doses eradicates ALDH$^+$ CSCs in TNBC overexpressing NQO1 through apoptotic death.

To verify if IB-DNQ alone or together with ATN224 triggers apoptotic death in NQO1^{lo} TNBC cells, we treated SUM149 cells with 25 to 100 nmol/L of IB-DNQ alone or together with ATN224 (5 μmol/L) for 20 hours. Following treatment, SUM149 cells were harvested, labeled with Annexin V–APC and DAPI, and analyzed by flow cytometry (**Fig. 4C**, left). Although IB-DNQ (25–100 nmol/L) or ATN224 (5 μmol/L) alone did not generate detectable apoptosis, the addition of ATN224 plus 25 to 100 nmol/L of IB-DNQ markedly induced early and late apoptosis of SUM149 breast cancer cells (**Fig. 4C**, right). Treatment with a sublethal dose of IB-DNQ in combination with ATN224 synergistically induced TUNEL$^+$ apoptotic death in ALDH$^+$ CSCs (arrows) and ALDH$^-$ bulk tumor cells (**Fig. 4D,** arrowheads).

IB-DNQ plus ATN224 synergistically enhances MitoROS production and loss of mitochondrial membrane potential

As NQO1-mediated redox cycling induces tumor cell killing via oxidant stress, we next measured the levels of cellular ROS by CellROX labeling and MitoROS by MitoSOX labeling with flow cytometry. IB-DNQ significantly increased total ROS (**Fig. 5A–C**) and MitoROS (**Fig. 5D–F**) in a dose-dependent fashion in Vari068, SUM159, and SUM149 breast cancer cells. Similar to increased levels of total ROS and MitoROS, IB-DNQ significantly increased the levels of cellular superoxide in SUM159 (Supplementary Fig. S6B) and SUM149 (Supplementary Fig. S6C) breast cancer cells. When these cells were treated with sublethal doses of IB-DNQ plus ATN224 (5 μmol/L), cellular ROS (**Fig. 5A–C**), superoxide (Supplementary Fig. S6B and S6C), and MitoROS (**Fig. 5D–F**; Supplementary Fig. S6D–S6F) were markedly increased when compared

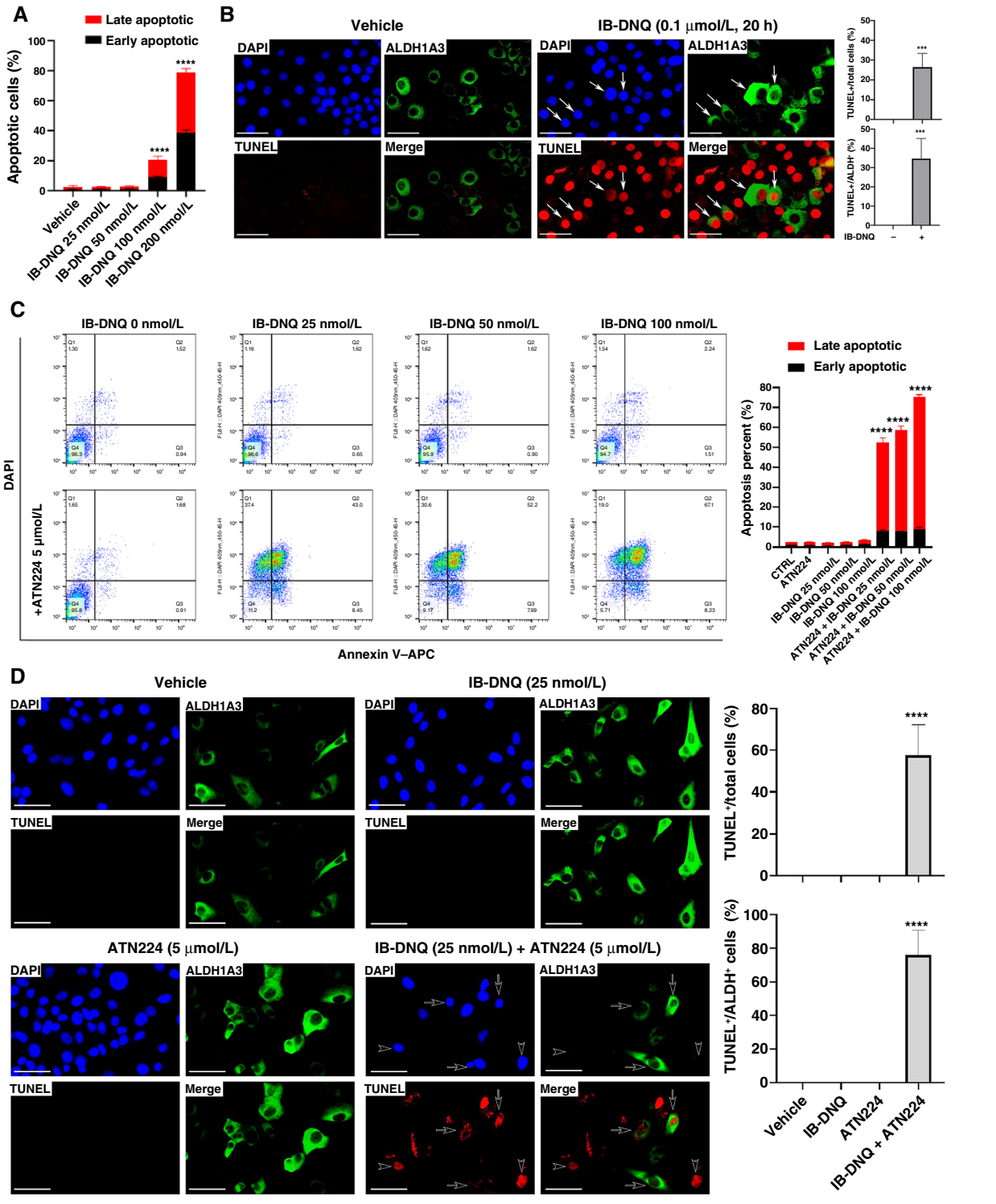

Figure 4.

IB-DNQ induces apoptosis of Vari068 ALDH$^+$ CSCs, and ATN224 enhances IB-DNQ–mediated apoptosis in SUM149 breast cancer cells expressing low/modest levels of NQO1. **A** and **B,** Vari068 cells treated with IB-DNQ for 20 hours were examined by flow cytometry to assess early and late apoptotic cells (**A**), or fixed and examined by ALDH1A3 and TUNEL dual labeling fluorescent microscopy (**B**) and percentage of TUNEL$^+$ over total or ALDH1A3$^+$ cells was scored in three different areas. **C** and **D,** SUM149 cells treated with IB-DNQ alone or together with ATN224 (5 μmol/L) for 20 hours were examined by flow cytometry to detect early and late apoptotic cells (**C**), or fixed and examined by ALDH1A3 and TUNEL dual labeling (**D**), and percentage of TUNEL$^+$ over total or ALDH1A3$^+$ cells was scored in three different areas. ***, $P < 0.001$; ****, $P < 0.0001$ vs. vehicle. $n = 3$, one-way ANOVA for **A** and **C** and unpaired Student t test for **B** and **D**. Scale bar, 50 μm.

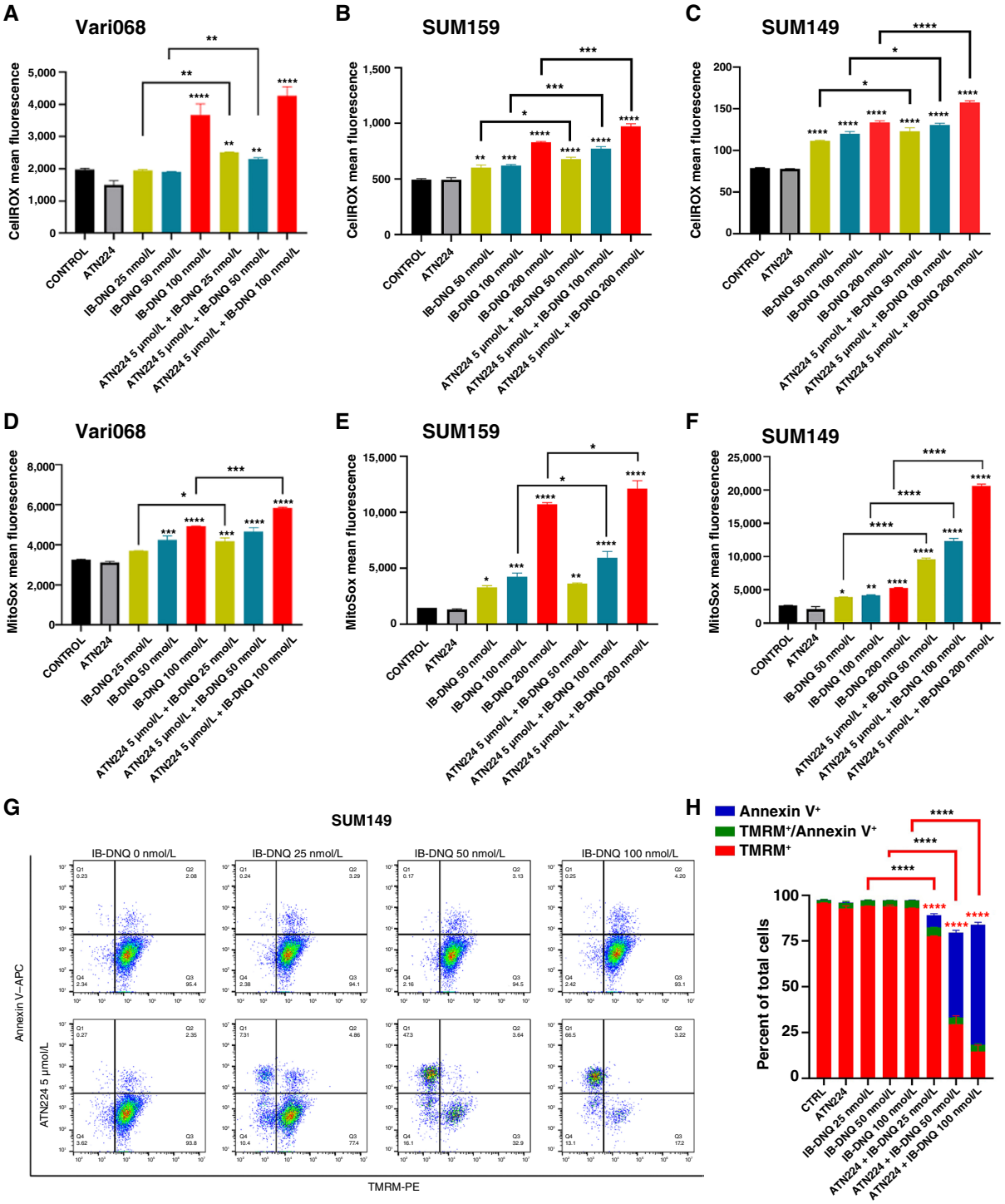

Figure 5.

IB-DNQ in combination with ATN224 synergistically enhances total ROS and MitoROS production, resulting in the loss of mitochondrial membrane potential. **A–F,** Vari068, SUM159, and SUM149 cells were treated with control (DMSO), ATN224 (5 μmol/L), IB-DNQ alone, or IB-DNQ plus ATN224 for 20 hours and examined by CellROX (**A–C**) or MitoSOX (**D–F**) labeling, followed by flow cytometry. **G** and **H,** SUM149 cells treated with IB-DNQ (0–100 nmol/L) alone or together with 5 μmol/L of ATN224 for 20 hours were stained with Annexin V–APC plus TMRM-PE and examined by flow cytometry (**G**), and percentage of $TMRM^+$, $TMRM^+$Annexin V^+ and Annexin V^+ cells was plotted (**H**). *, $P < 0.05$; **, $P < 0.01$; ***, $P < 0.001$; ****, $P < 0.0001$ vs. control or indicated by brackets; $n = 3$, one-way ANOVA for **A–F** and **H**.

with cells treated with IB-DNQ alone, and this increase is more prominent in NQO1^{lo} SUM149 breast cancer cells.

To further explore if increased MitoROS promotes mitochondrial oxidative damage, triggering the intrinsic apoptosis pathway, we measured mitochondrial membrane potential (by TMRM labeling) and apoptosis (by Annexin V labeling) in SUM149 cells treated with sublethal doses of IB-DNQ alone, or together with ATN224 (**Fig. 5G**). This revealed that IB-DNQ (25–100 nmol/L) or ATN224 (5 μmol/L) alone is not sufficient to induce significant loss of mitochondrial membrane potential and apoptosis. However, in the presence of ATN224, IB-DNQ induces the loss of mitochondrial membrane potential and increases apoptosis in a dose-dependent fashion (**Fig. 5H**).

NQO1 resides in the mitochondrial IMS driving IB-DNQ futile redox cycling, leading to excessive levels of MitoROS and mitochondrial oxidative damage

The findings described above suggest that IB-DNQ may directly target mitochondria in ALDH$^+$ CSCs to induce apoptosis. Notably, SOD1 localizes in the cytoplasm and mitochondrial IMS, where it provides major dismutase activity to protect mitochondrial integrity of breast cancer cells (59). We hypothesize that a portion of NQO1 localizes in the mitochondria, where it coresides with SOD1 in the mitochondrial IMS. Therefore, SOD1 inhibition, by augmenting MitoROS production from IB-DNQ, potentiates mitochondrial oxidative injury to activate mitochondrial apoptotic pathway.

To determine the subcellular localization of NQO1, we purified mitochondrial and cytosol fractions from NQO1^{med} (SUM159) and NQO1^{lo} (SUM149 and HCC1806) TNBC cells and examined NQO1 and SOD1 expression in each fraction. In addition to cytosolic localization, significant portions of NQO1 and SOD1 are both localized to the mitochondria fraction (**Fig. 6A**). By contrast, the mitochondrial protein succinate dehydrogenase complex subunit A is exclusively localized to the mitochondrial fraction, whereas S-phase kinase-associated protein 1, a cytosolic protein, is exclusively localized in the cytosol fraction (**Fig. 6A**). We also performed cell fractionation using a panel of NQO1^{hi} breast cancer cells, including Vari068, MDA-MB-436, MDA-MB-453, MCF7, and ZR-75-1. This revealed that, in addition to cytosolic NQO1, a significant portion of NQO1 is localized in the mitochondrial fraction in each breast cancer cell line examined (**Fig. 6B**). In contrast to NQO1, two mitochondrial proteins succinate dehydrogenase complex subunit A and voltage-dependent anion channel are exclusively localized to the mitochondrial fraction, whereas S-phase kinase-associated protein-1 is exclusively localized in the cytosol fraction. Therefore, NQO1-mediated futile redox cycling may occur not only in the cytosol but also in the mitochondria.

To assess colocalization of NQO1 and Cyto c, a protein known to reside in the mitochondrial IMS, we performed confocal microscopy of SUM159 breast cancer cells subjected to dual-color immunofluorescent staining with NQO1 and Cyto c–specific antibodies. This revealed that a significant portion of NQO1 colocalizes with Cyto c in the mitochondrial IMS (**Fig. 6C**, **a–c**). Furthermore, volume assay of NQO1 and Cyto c labeling from a specific angle using Volume Viewer of the NIS-Elements Viewer software confirmed that NQO1 colocalizes with Cyto c in the mitochondria (**Fig. 6C, d–f**).

To test if IB-DNQ futile redox cycling generates mitochondrial oxidative damage, we treated NQO1^{hi} Vari068 breast cancer cells with 100 nmol/L of IB-DNQ for 0, 2, 4, and 8 hours and determined the effect of IB-DNQ on mitochondrial morphology using transmission electron microscopy. Compared with control (DMSO)-treated cells, which display typical mitochondrial morphology with intact cristae, Vari068 cells treated with IB-DNQ exhibit gradual loss of cristae and dilated/vacuolized mitochondria (**Fig. 6D**), indicative of mitochondrial oxidative damage. Similar transmission electron microscopy studies were performed on NQO1^{lo} SUM149 breast cancer cells treated with mock (DMSO), IB-DNQ (100 nmol/L), ATN224 (5 μmol/L), or IB-DNQ and ATN224 for 16 hours. Co-treatment with IB-DNQ and ATN224 generates a synergy in producing mitochondrial oxidative damage, manifested by the loss of cristae and dilated/vacuolized mitochondria, although treatment with IB-DNQ alone had no effect (**Fig. 6E**). Inhibition of SOD1 with ATN224 produces mild mitochondrial oxidative damage manifested by some degree of cristae loss and mitochondrial vacuolization (**Fig. 6E**), consistent with a previous study (59).

Given the role of IB-DNQ redox cycling in targeting the mitochondria to produce oxidative stress in TNBC cells, we next determined if IB-DNQ impairs mitochondrial oxidative metabolism and ATP biosynthesis. Treatment of SUM159 breast cancer cells with IB-DNQ (at 300 nmol/L) for 2 hours did not affect cell survival (Supplementary Fig. S7A), but significantly inhibited extracellular oxygen consumption (**Fig. 6F**) and intracellular ATP levels (**Fig. 6G**), suggesting a role of IB-DNQ in suppressing mitochondrial respiration and ATP production.

NQO1-mediated futile redox cycling from IB-DNQ results in the release of mitochondrial Cyto c and activation of caspase-3–mediated apoptosis

To test if IB-DNQ promotes Cyto c release from mitochondrial IMS, initiating the mitochondrial apoptotic pathway (62), we used 100 nmol/L of IB-DNQ to treat NQO1^{hi} Vari068 breast cancer cells for 0 to 12 hours and conducted cell fractionation to isolate the mitochondrial and cytosol fractions at each time point. IB-DNQ gradually induces the loss of Cyto c from the mitochondria, accompanied by increased Cyto c in the cytosol (**Fig. 6H**). Interestingly, compared with vehicle-treated cells, treatment of NQO1^{lo} SUM149 cells with IB-DNQ at 100 nmol/L or ATN224 at 5 μmol/L for 16 hours significantly increased mitochondrial Cyto c protein expression (**Fig. 6I**). This suggests that IB-DNQ or ATN224 treatment is sufficient to increase mitochondrial oxidative stress in SUM149, leading to mitochondrial antioxidant responses by boosting Cyto c expression, as Cyto c itself serves as an antioxidant protein (63). However, when SUM149 cells were treated with IB-DNQ plus ATN224, the enhanced mitochondrial Cyto c expression was lost (**Fig. 6I**), accompanied by significantly increased Cyto c in the cytosol fraction (**Fig. 6I**).

We investigated the downstream molecular mechanisms associated with Cyto c release. Treatment with IB-DNQ dose-dependently induced the cleavage of caspase-3 (Casp3), accompanied by the cleavage of its substrate PARP, and decreased BCL2 and BCL-XL (antiapoptotic); however, increased BIM and p-H2A.X (proapoptotic) expression in NQO1^{hi} Vari068 breast cancer cells (**Fig. 6J**). In NQO1^{lo} SUM149 breast cancer cells, treatment with IB-DNQ (100 nmol/L) or ATN224 (5 μmol/L) each had no effect on Casp3 activation, PARP cleavage, and BCL2/BCL-XL or BIM/p-H2A.X expression. However, cotreatment with IB-DNQ and ATN224 synergistically enhanced Casp3 activation and PARP cleavage, associated with reduced BCL2/BCL-XL, but increased BIM and p-H2A.X expression (**Fig. 6K**). IB-DNQ treatment of SUM159 breast cancer cells also triggered Casp3 activation and PARP cleavage, associated with reduced BCL2 and increased BIM expression, and treatment with ATN224 + IB-DNQ significantly augmented the efficacy of IB-DNQ in promoting Casp3 and PARP

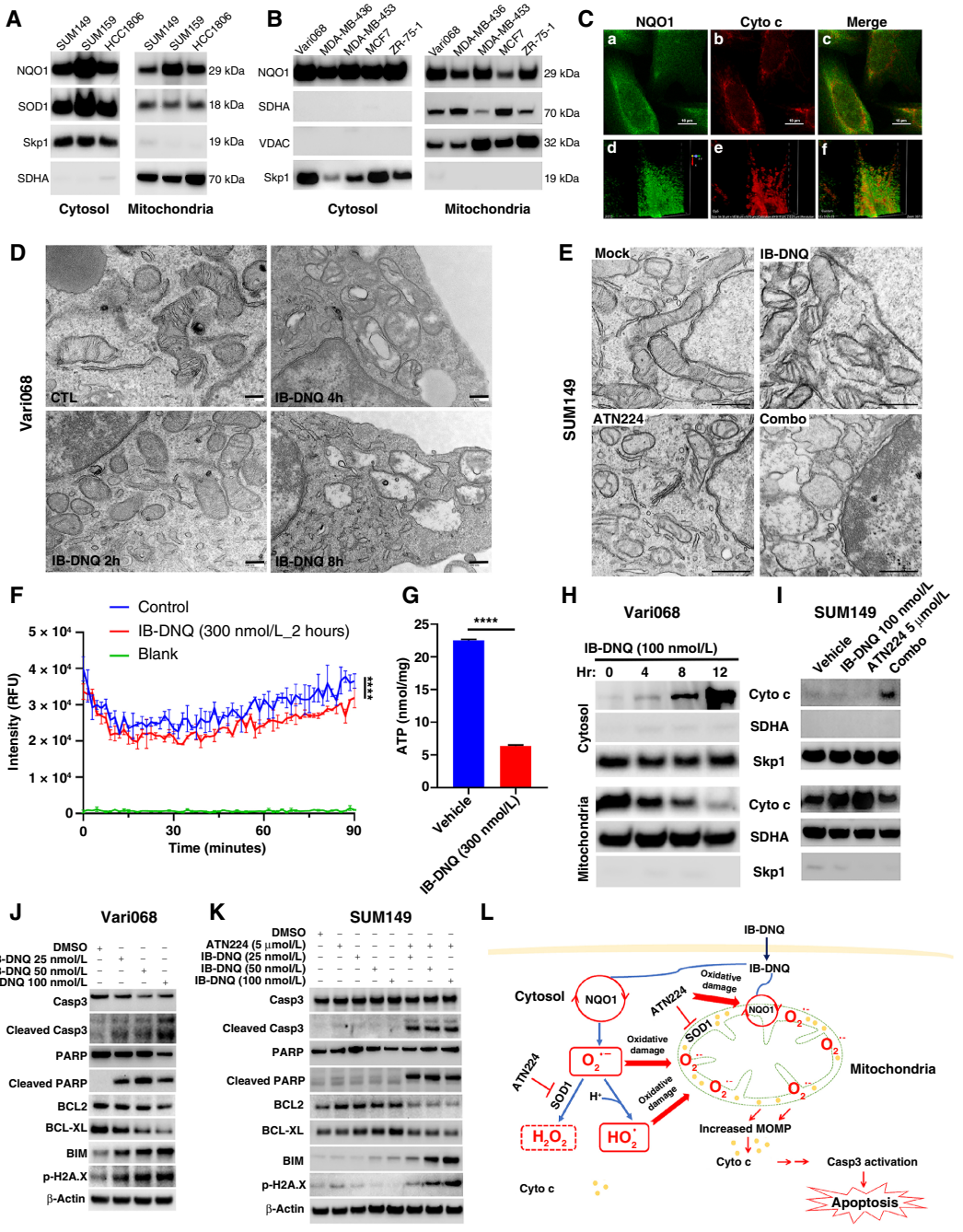

Figure 6.

NQO1 residing in the mitochondrial IMS drives IB-DNQ redox cycling, promoting mitochondrial oxidative damage, Cyto c release, and activation of Casp3-mediated mitochondrial apoptotic pathway. **A** and **B,** NQO1^{med} and NQO1^{lo} (**A**) and NQO1^{hi} (**B**) TNBC cells were examined for NQO1, SOD1, succinate dehydrogenase complex subunit A (SDHA), and S-phase kinase-associated protein-1 (Skp1) expression in the mitochondrial and cytosol fraction. **C,** SUM159 cells labeled with specific antibodies against NQO1 and Cyto c were examined by confocal microscopy. Scale bar, 120 μm. **D** and **E,** Vari068 and SUM149 cells treated with 100 nmol/L of IB-DNQ for 0 to 8 hours (**D**) or with vehicle, IB-DNQ (100 nmol/L), ATN224 (5 μmol/L), IB-DNQ plus ATN224 for 16 hours (**E**) were processed and examined by transmission electron microscopy. Bars, 200 (**D**) and 500 (**E**) nm. **F,** SUM159 cells were treated with vehicle or IB-DNQ for 2 hours and measured for oxygen consumption based on fluorescent intensity (RFU) of an oxygen-bleaching fluorescent dye in the media covered by mineral oil at 1.5 minutes intervals for 90 minutes. ****, $P < 0.0001$ ($n = 3$, two-way ANOVA). **G,** ATP levels in the lysates of SUM159 cells treated with vehicle or IB-DNQ for 2 hours were measured and normalized by protein concentrations. ****, $P < 0.0001$ with unpaired Student t test ($n = 3$). **H** and **I,** Vari068 and SUM149 cells treated with IB-DNQ (100 nmol/L) for 0 to 12 hours (**H**) or IB-DNQ and ATN224 alone or in combination for 16 hours (**I**) were used to isolate mitochondrial and cytosol fractions and examine Cyto c, SDHA, and Skp1 expression. **J** and **K,** Lysates of Vari068 (**J**) and SUM149 (**K**) cells treated with IB-DNQ alone or IB-DNQ plus ATN224 for 20 hours were subjected to immunoblotting to examine the expression of apoptosis-related proteins. **L,** A model illustrating the mechanisms of action for IB-DNQ–mediated prooxidant therapy targeting TNBC cells including CSCs. MOMP, mitochondrial outer membrane permeability.

cleavage, the reduction of BCL2, and induction of BIM expression (Supplementary Fig. S7B). Inhibition of Casp3 with Z-DEVD-FMK in SUM159 breast cancer cells significantly rescued IB-DNQ–induced cell lethality, whereas ferrostatin-1, an inhibitor of ferroptosis, failed to significantly rescue this lethality (Supplementary Fig. S7C). Parallel with the rescue of IB-DNQ–induced cell lethality, Z-DEVD-FMK partially but significantly rescued the decreased proportion of $ALDH^+$ CSCs in SUM159 treated with IB-DNQ (Supplementary Fig. S7D). These studies suggest a novel mechanism of action for NQO1-mediated futile redox cycling from IB-DNQ in killing TNBC cells including CSCs (**Fig. 6L**), where a significant portion of NQO1 and SOD1 both reside in the mitochondrial IMS, and SOD1 inhibition synergizes with IB-DNQ redox cycling to abrogate CSCs and bulk tumor cells by augmenting mitochondrial oxidative injury, resulting in Cyto c release and activation of Casp3-mediated apoptosis.

IB-DNQ alone or together with SOD1 inhibition inhibits tumor growth, metastasis, and tumor-initiating potential of TNBC xenografts

To test the feasibility of using IB-DNQ as an antitumor therapy for TNBC cells overexpressing NQO1, we injected Vari068 breast cancer cells into the fourth MFP of SCID mice and treated tumor-bearing mice with vehicle (20% HPβCD) or IB-DNQ (10 mg/kg, i.v.) for 2 weeks as outlined in **Fig. 7A**. This treatment regime had no significant effect on mouse body weight (**Fig. 7B**), confirming low toxicity of IB-DNQ. Monitoring tumor growth after the last treatment for 2 weeks indicated that IB-DNQ significantly inhibited primary tumor growth (**Fig. 7C**), and examination of lung histology from each group of mice revealed that IB-DNQ treatment markedly suppressed lung metastatic tumor nodule formation (**Fig. 7D**). Further IHC staining revealed that IB-DNQ induced Casp3 cleavage, whereas Ki67 staining was not significantly changed (**Fig. 7E**), suggesting that IB-DNQ suppresses tumor growth and metastasis formation by promoting apoptotic death.

To further validate the effectiveness of IB-DNQ alone or together with SOD1 inhibition on tumor growth and tumor-initiating potential in xenograft models of TNBC expressing low/modest levels of NQO1, we injected SUM149 breast cancer cells into the fourth MFP of SCID mice and treated tumor-bearing mice intravenously with vehicle (20% HPβCD), IB-DNQ (10 mg/kg), ATN224 (10 mg/kg), and IB-DNQ (10 mg/kg) + ATN224 (10 mg/kg) for 3 weeks as outlined in **Fig. 7F**. Single or combination therapy with IB-DNQ and ATN224 had no significant effect on mouse body weight (**Fig. 7G**), suggesting that combination of IB-DNQ and ATN224 did not generate added toxicity. By monitoring tumor growth after treatment initiation for 5 weeks indicated that IB-DNQ alone did not significantly inhibit primary tumor growth, whereas ATN224 modestly inhibited the growth of SUM149 breast cancer cells. In contrast to IB-DNQ or ATN224 alone, combination treatment with IB-DNQ plus ATN224 generated a synergistic effect in suppressing mammary tumor growth (**Fig. 7H**). Examination of tumor weight in each group of mice at the end of tumor monitoring confirmed that treatment with IB-DNQ plus ATN224 significantly reduced residual tumor weight (**Fig. 7I**). Furthermore, limiting-dilution transplantation studies in secondary SCID mice using dissociated $H2Kd^-$ live tumor cells from residual tumors revealed that treatment with ATN224 but not IB-DNQ was able to decrease tumor-initiating potential, and treatment with ATN224 plus IB-DNQ had the most significant effect in reducing tumor-initiating potential of residual tumor cells (**Table 1**).

As a copper-chelating inhibitor of SOD1, ATN224 may inhibit other copper/zinc proteins that are involved in angiogenesis (64–66) and mitochondrial oxidative phosphorylation (67), confounding a specific role of SOD1 inhibition in synergizing IB-DNQ redox cycling to suppress tumor growth and CSC activity. To address this issue, we injected SUM149 breast cancer cells expressing Dox-inducible KD (shSOD1) or scrambled control (SCR) into the fourth MFP of female SCID mice, and mice bearing mammary tumors expressing shSOD1 or SCR were each randomized into two groups and subjected to treatment with Dox (200 μg/mL in water) plus vehicle (20% HPβCD, i.v.) or IB-DNQ (10 mg/kg, i.v.) for 3 weeks as indicated in the treatment regime (Supplementary Fig. S8A). Consistent with the study performed with parent SUM149 breast cancer cells (**Fig. 7H**), mice bearing tumor cells expressing the SCR did not exhibit significant tumor growth retardation after IB-DNQ treatment (Supplementary Fig. S8B). In contrast to the modest effect of ATN224 in suppressing SUM149 tumor growth (**Fig. 7H**), Dox-induced KD of SOD1 significantly inhibited tumor growth, and IB-DNQ treatment further enhanced tumor growth retardation of SOD1 KD cells (Supplementary Fig. S8B). Together, these studies suggest that IB-DNQ redox cycling serves as a feasible approach targeting TNBC overexpressing NQO1, and SOD1 inhibition greatly augments antitumor efficacy of this prooxidant strategy in TNBC cells expressing low or modest levels of NQO1. Furthermore, this approach is able to target CSCs that are resistant to conventional therapies.

Discussion

In this study, we examined the antitumor efficacy and mechanism of action of IB-DNQ alone or in combination with SOD1 inhibition in abrogating CSCs in TNBC expressing different levels of NQO1. We demonstrate that a significant portion of NQO1 and SOD1 are localized in the mitochondria, and genetic or pharmacologic inhibition of SOD1 synergizes with NQO1-bioactivated redox cycling from IB-DNQ to elicit CSC lethality by augmenting mitochondrial oxidative injury, leading to Cyto c release and activation of Casp3-mediated mitochondrial apoptotic pathway.

Through the study, we identified two antioxidant enzymes NQO1 and SOD1 as therapeutic vulnerabilities of $ALDH^+$ E-CSCs and $CD24^{-/lo}CD44^{+/hi}$ M-CSCs in TNBC. Dox-inducible KD of NQO1 in $NQO1^{hi}$ Vari068 preferentially decreases $ALDH^+$ E-CSCs, whereas Dox-inducible KD of SOD1 in $NQO1^{lo}$ SUM149 selectively abrogates $CD24^{-/lo}CD44^{+/hi}$ M-like CSCs. Of note, targeting NQO1 with sub-lethal doses of IB-DNQ preferentially abrogates $ALDH^+$ E-CSCs in TNBC expressing high levels of NQO1 (i.e., Vari068 and SUM159). However, for TNBC cells expressing modest/low levels of NQO1 (i.e., SUM149), the efficacy of IB-DNQ targeting $ALDH^+$ E-CSCs but not $CD24^-CD44^+$ M-CSCs is significantly decreased because of lower sensitivity of E-CSCs (vs. M-CSCs) to the modest levels of ROS elicited by IB-DNQ. We show that SOD1 is highly expressed in all TNBC cell lines examined, and genetic or pharmacological inhibition of SOD1, but not CAT or SOD2, markedly enhances IB-DNQ–elicited MitoROS production and killing of CSCs in both E and M states. Thus, SOD1 overexpression provides a therapeutic window for CSCs in TNBC with modest/low levels of NQO1 expression.

We confirmed *in vitro* and in TNBC xenograft models that combined treatment with IB-DNQ and SOD1 inhibition renders both BCSCs and bulk tumor cells more sensitive to IB-DNQ–elicited

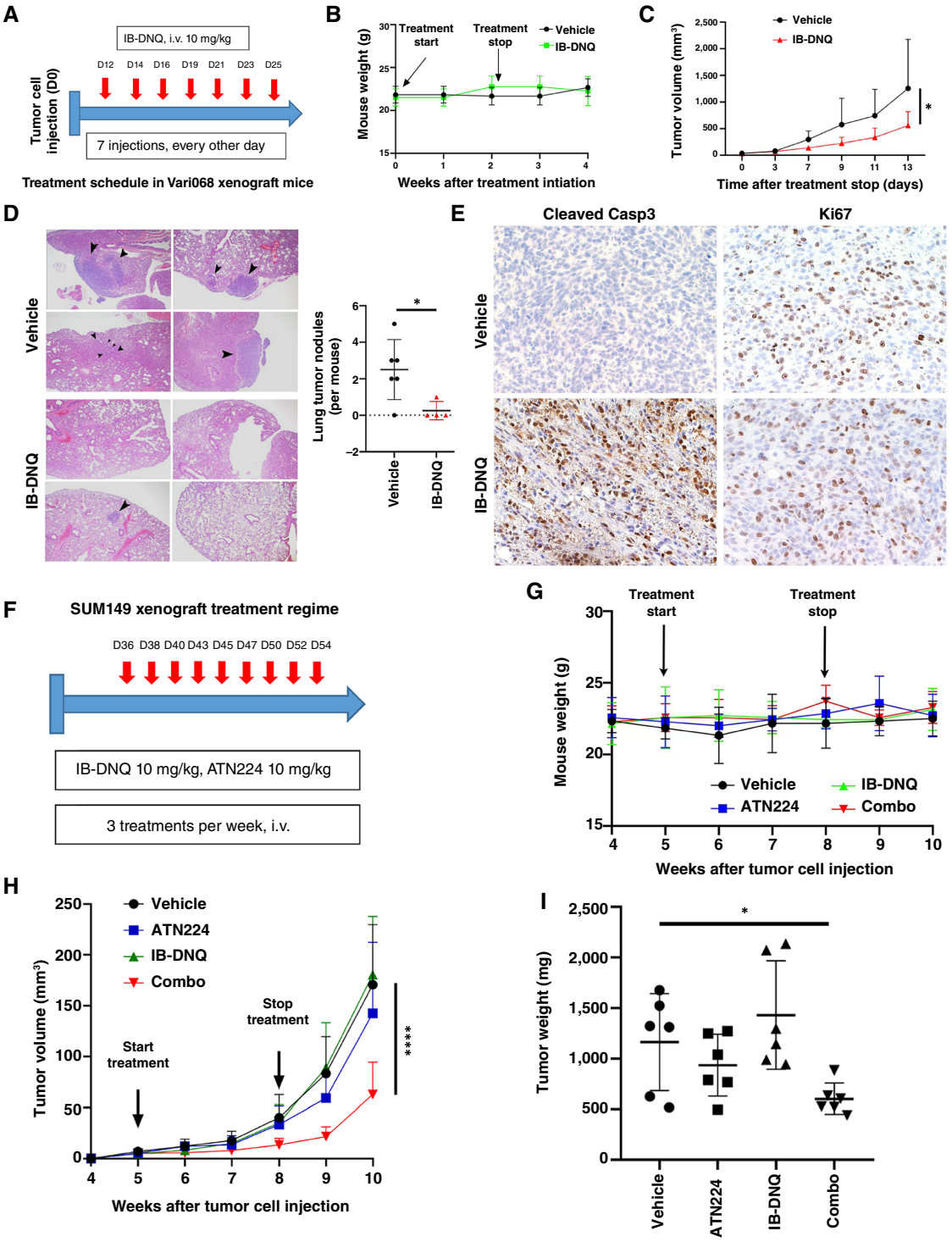

Figure 7.

IB-DNQ alone or together with SOD1 inhibition suppresses tumor growth, metastasis, and tumor-initiating potential of TNBC xenografts. **A–C,** Vari068 mammary tumor xenograft mice were randomized and treated with vehicle or IB-DNQ as indicated in **A**. **B** and **C,** Mouse body weight was examined weekly for 4 weeks after treatment initiation (**B**) and mammary tumor growth following the last treatment was monitored for 2 weeks (**C**). *, $P < 0.05$ ($n = 6$). **D,** Lung histologic sections from each group of mice were harvested to examine metastatic tumor nodule formation. *, $P < 0.05$. **E,** staining of tumor sections treated with IB-DNQ vs. vehicle using antibodies against cleaved Casp3 or Ki67. **F** and **H,** SUM149 mammary tumor xenograft mice were randomized into four groups and treated with the regime indicated in **F**, and mouse body weight (**G**) and mammary tumor growth (**H**) were examined weekly for 6 weeks. ****, $P < 0.0001$ (vs. vehicle or IB-DNQ, $n = 6$). **I,** Tumor weight for each group of mice at the end of tumor monitoring. *, $P < 0.05$ (vehicle vs. combo, $n = 6$). **C** and **H,** Two-way ANOVA; **D** and **I,** two-tailed Student t test.

Table 1. Limiting-dilution transplantation in secondary SCID mouse.

	Tumors/injection sites				
Cells injected	**50,000**	**5,000**	**500**	**TIC frequency**	***P* value (vs. vehicle)**
Vehicle	8/8	8/8	6/8	1/152	
IB-DNQ	8/8	8/8	2/8	1/546	0.055
ATN224	8/8	5/8	3/8	1/1,586	0.0002
Combination	5/8	1/6	0/6	1/20,391	2.6e–15

lethality. As CSCs can be generated from bulk tumor cells under chemotherapeutic stress through the "dedifferentiation" process, simultaneously targeting CSCs and bulk differentiated tumor cells by IB-DNQ–based futile redox cycling will be a promising therapeutic approach for advanced breast cancer such as TNBC. Our data in TNBC xenograft models and a recent study in feline oral squamous cell carcinoma (56) suggest that IB-DNQ is well tolerated, consistent with other studies showing that β-Lap produced only mild toxicity (anemia and possible methemoglobinemia) in a phase I clinical trial (52). In addition, the SOD1 inhibitor ATN224 is orally available and was well tolerated in a phase 1 study of patients with advanced solid cancers (68), and a derivative of ATN224, tetrathiomolybdate is FDA approved to treat Wilson disease. These preclinical and clinical results suggest that combination therapy using IB-DNQ and ATN224 or tetrathiomolybdate will be well tolerated in patients with TNBC.

Previous studies from our group and others have demonstrated that proliferative $ALDH^+$ CSCs are highly reliant on mitochondrial oxidative metabolism (36, 37, 69), providing a rationale for targeting mitochondrial vulnerabilities to eradicate this CSC population. We show here that targeting NQO1 by IB-DNQ at sublethal doses is sufficient to trigger apoptosis of $ALDH1A3^+$ E-CSCs in TNBC overexpressing NQO1 and that pharmacologic inhibition of SOD1, by enhancing MitoROS production, greatly enhances IB-DNQ–induced loss of mitochondrial membrane potential and apoptosis of $ALDH1A3^+$ CSCs. These data strongly suggest that IB-DNQ redox cycling from NQO1 directly targets mitochondria in $ALDH^+$ CSCs, triggering the intrinsic apoptotic pathway.

As increased ROS stress promotes the conversion of $CD24^{-/lo}CD44^{+/hi}$ M-CSCs to more proliferative $ALDH^+$ E-CSCs (37), by targeting two elevated antioxidant enzymes NQO1 and SOD1 via IB-DNQ mitochondrial futile redox cycling, this study provides a novel therapeutic strategy effectively targeting CSCs including $ALDH^+$ E-CSCs and $CD24^{-/lo}CD44^{+/hi}$ M-CSCs in TNBC. By promoting the conversion of $CD24^{-/lo}CD44^{+/hi}$ M-CSCs to $ALDH^+$ E-CSCs and effectively inducing apoptosis in the later, our prooxidant strategy described in this study is able to target CSCs across the EMT–MET continuum. Because NQO1 and SOD1 are overexpressed in many other malignancies, this CSC-targeting strategy may have wide applicability.

A limitation of this study is the use of xenograft models of TNBC established in immunodeficient SCID mice to validate the antitumor efficacy of targeting NQO1 and SOD1 through IB-DNQ mitochondrial futile redox cycling. This animal model is appropriate to assess the efficacy of this strategy directly on CSCs and bulk tumor cells. However, other NBRCC such as β-Lap has been shown to play a role in promoting host antitumor immunity (55). As the host immune system plays important roles in regulating CSCs and therapeutic responses, future studies are necessary to assess if and how this futile oxidant–generating strategy using IB-DNQ alone or together with SOD1 inhibitors eradicates CSCs and bulk tumor cells in immunocompetent mouse models. This limitation should be considered when interpreting the results and translating to patients.

Authors' Disclosures

P.J. Hergenrother reports personal fees from Vanquish Oncology, Systems Oncology, Oncoteq, and Arrepath outside the submitted work, as well as US patent 9233960 issued. No disclosures were reported by the other authors.

Authors' Contributions

M. Luo: Conceptualization, data curation, formal analysis, supervision, funding acquisition, validation, investigation, visualization, writing–original draft, project administration, writing–review and editing. **N. Shen:** Data curation, formal analysis, validation, investigation, visualization, methodology. **L. Shang:** Data curation, formal analysis, investigation. **Z. Fang:** Formal analysis, validation, investigation. **Y. Xin:** Validation, investigation. **Y. Ma:** Validation, investigation. **M. Du:** Validation, investigation. **Y. Yuan:** Formal analysis, investigation. **C. Hu:** Formal analysis, investigation. **Y. Tang:** Formal analysis, validation. **J. Huang:** Formal analysis, investigation. **W. Wei:** Conceptualization, funding acquisition. **M.R. Lee:** Resources. **P.J. Hergenrother:** Resources, funding acquisition, writing–review and editing. **M.S. Wicha:** Supervision, funding acquisition, writing–review and editing.

Acknowledgments

This research was supported by NIH R35 CA197585, R01 CA28298-01A1, and BCRF-22-173 (to M.S. Wicha); NIH R01 DE026836 and R35 CA283859 (to P.J. Hergenrother); National Science Foundation of China (nos. 82373084 and 82103385); Shenzhen High-Level Hospital Construction Fund; Peking University Shenzhen Hospital Scientific Research Fund (KYQD2023256); Shenzhen San-Ming Project (SZSM201612010); and Shenzhen Key Medical Discipline Construction Fund (SZXK017).

Note

Supplementary data for this article are available at Cancer Research Online (http://cancerres.aacrjournals.org/).

Received March 9, 2024; revised July 24, 2024; accepted September 6, 2024; published first September 12, 2024.

References

1. Garrido-Castro AC, Lin NU, Polyak K. Insights into molecular classifications of triple-negative breast cancer: improving patient selection for treatment. Cancer Discov 2019;9:176–98.
2. Loizides S, Constantinidou A. Triple negative breast cancer: immunogenicity, tumor microenvironment, and immunotherapy. Front Genet 2022;13:1095839.

3. Charafe-Jauffret E, Ginestier C, Iovino F, Wicinski J, Cervera N, Finetti P, et al. Breast cancer cell lines contain functional cancer stem cells with metastatic capacity and a distinct molecular signature. Cancer Res 2009;69:1302–13.
4. Abdoli Shadbad M, Hosseinkhani N, Asadzadeh Z, Derakhshani A, Karim Ahangar N, Hemmat N, et al. A systematic review to clarify the prognostic values of CD44 and $CD44^{+}CD24^{-}$ phenotype in triple-negative breast cancer patients: lessons learned and the road ahead. Front Oncol 2021;11:689839.
5. Olsson M, Larsson P, Johansson J, Sah VR, Parris TZ. Cancer stem cells are prevalent in the basal-like 2 and mesenchymal triple-negative breast cancer subtypes in vitro. Front Cell Dev Biol 2023;11:1237673.
6. Shafee N, Smith CR, Wei S, Kim Y, Mills GB, Hortobagyi GN, et al. Cancer stem cells contribute to cisplatin resistance in Brca1/p53-mediated mouse mammary tumors. Cancer Res 2008;68:3243–50.
7. Li X, Lewis MT, Huang J, Gutierrez C, Osborne CK, Wu M-F, et al. Intrinsic resistance of tumorigenic breast cancer cells to chemotherapy. J Natl Cancer Inst 2008;100:672–9.
8. Diehn M, Cho RW, Lobo NA, Kalisky T, Dorie MJ, Kulp AN, et al. Association of reactive oxygen species levels and radioresistance in cancer stem cells. Nature 2009;458:780–3.
9. Croker AK, Allan AL. Inhibition of aldehyde dehydrogenase (ALDH) activity reduces chemotherapy and radiation resistance of stem-like $ALDHhiCD44^{+}$ human breast cancer cells. Breast Cancer Res Treat 2012;133:75–87.
10. Tanei T, Morimoto K, Shimazu K, Kim SJ, Tanji Y, Taguchi T, et al. Association of breast cancer stem cells identified by aldehyde dehydrogenase 1 expression with resistance to sequential paclitaxel and epirubicin-based chemotherapy for breast cancers. Clin Cancer Res 2009;15:4234–41.
11. Phillips TM, McBride WH, Pajonk F. The response of $CD24(^{-}/low)/CD44^{+}$ breast cancer-initiating cells to radiation. J Natl Cancer Inst 2006;98:1777–85.
12. Lu H, Samanta D, Xiang L, Zhang H, Hu H, Chen I, et al. Chemotherapy triggers HIF-1-dependent glutathione synthesis and copper chelation that induces the breast cancer stem cell phenotype. Proc Natl Acad Sci U S A 2015;112:E4600–9.
13. Lu H, Xie Y, Tran L, Lan J, Yang Y, Murugan NL, et al. Chemotherapy-induced S100A10 recruits KDM6A to facilitate OCT4-mediated breast cancer stemness. J Clin Invest 2020;130:4607–23.
14. Echeverria GV, Ge Z, Seth S, Zhang X, Jeter-Jones S, Zhou X, et al. Resistance to neoadjuvant chemotherapy in triple-negative breast cancer mediated by a reversible drug-tolerant state. Sci Transl Med 2019;11:eaav0936.
15. Dhanyamraju PK, Schell TD, Amin S, Robertson GP. Drug-tolerant persister cells in cancer therapy resistance. Cancer Res 2022;82:2503–14.
16. Pu Y, Li L, Peng H, Liu L, Heymann D, Robert C, et al. Drug-tolerant persister cells in cancer: the cutting edges and future directions. Nat Rev Clin Oncol 2023;20:799–813.
17. Al-Hajj M, Wicha MS, Benito-Hernandez A, Morrison SJ, Clarke MF. Prospective identification of tumorigenic breast cancer cells. Proc Natl Acad Sci U S A 2003;100:3983–8.
18. Ginestier C, Hur MH, Charafe-Jauffret E, Monville F, Dutcher J, Brown M, et al. ALDH1 is a marker of normal and malignant human mammary stem cells and a predictor of poor clinical outcome. Cell Stem Cell 2007;1:555–67.
19. Huang EH, Hynes MJ, Zhang T, Ginestier C, Dontu G, Appelman H, et al. Aldehyde dehydrogenase 1 is a marker for normal and malignant human colonic stem cells (SC) and tracks SC overpopulation during colon tumorigenesis. Cancer Res 2009;69:3382–9.
20. Carpentino JE, Hynes MJ, Appelman HD, Zheng T, Steindler DA, Scott EW, et al. Aldehyde dehydrogenase-expressing colon stem cells contribute to tumorigenesis in the transition from colitis to cancer. Cancer Res 2009;69:8208–15.
21. van den Hoogen C, van der Horst G, Cheung H, Buijs JT, Lippitt JM, Guzmán-Ramírez N, et al. High aldehyde dehydrogenase activity identifies tumor-initiating and metastasis-initiating cells in human prostate cancer. Cancer Res 2010;70:5163–73.
22. Sullivan JP, Spinola M, Dodge M, Raso MG, Behrens C, Gao B, et al. Aldehyde dehydrogenase activity selects for lung adenocarcinoma stem cells dependent on notch signaling. Cancer Res 2010;70:9937–48.
23. Liu S, Cong Y, Wang D, Sun Y, Deng L, Liu Y, et al. Breast cancer stem cells transition between epithelial and mesenchymal states reflective of their normal counterparts. Stem Cell Rep 2014;2:78–91.
24. Jolly MK, Somarelli JA, Sheth M, Biddle A, Tripathi SC, Armstrong AJ, et al. Hybrid epithelial/mesenchymal phenotypes promote metastasis and therapy resistance across carcinomas. Pharmacol Ther 2019;194:161–84.
25. Pastushenko I, Brisebarre A, Sifrim A, Fioramonti M, Revenco T, Boumahdi S, et al. Identification of the tumour transition states occurring during EMT. Nature 2018;556:463–8.
26. Luo M, Brooks M, Wicha MS. Epithelial-mesenchymal plasticity of breast cancer stem cells: implications for metastasis and therapeutic resistance. Curr Pharm Des 2015;21:1301–10.
27. Brooks MD, Burness ML, Wicha MS. Therapeutic implications of cellular heterogeneity and plasticity in breast cancer. Cell Stem Cell 2015;17:260–71.
28. Gupta PB, Pastushenko I, Skibinski A, Blanpain C, Kuperwasser C. Phenotypic plasticity: driver of cancer initiation, progression, and therapy resistance. Cell Stem Cell 2019;24:65–78.
29. Lu W, Kang Y. Epithelial-mesenchymal plasticity in cancer progression and metastasis. Dev Cell 2019;49:361–74.
30. Quintanal-Villalonga Á, Chan JM, Yu HA, Pe'er D, Sawyers CL, Sen T, et al. Lineage plasticity in cancer: a shared pathway of therapeutic resistance. Nat Rev Clin Oncol 2020;17:360–71.
31. Takebe N, Miele L, Harris PJ, Jeong W, Bando H, Kahn M, et al. Targeting Notch, Hedgehog, and Wnt pathways in cancer stem cells: clinical update. Nat Rev Clin Oncol 2015;12:445–64.
32. Yang L, Shi P, Zhao G, Xu J, Peng W, Zhang J, et al. Targeting cancer stem cell pathways for cancer therapy. Signal Transduct Target Ther 2020;5:8.
33. Dashzeveg NK, Taftaf R, Ramos EK, Torre-Healy L, Chumakova A, Silver DJ, et al. New advances and challenges of targeting cancer stem cells. Cancer Res 2017;77:5222–7.
34. Thankamony AP, Saxena K, Murali R, Jolly MK, Nair R. Cancer stem cell plasticity—a deadly deal. Front Mol Biosci 2020;7:79.
35. Luo M, Wicha MS. Targeting cancer stem cell redox metabolism to enhance therapy responses. Semin Radiat Oncol 2019;29:42–54.
36. Luo M, Wicha MS. Metabolic plasticity of cancer stem cells. Oncotarget 2015;6:35141–2.
37. Luo M, Shang L, Brooks MD, Jiagge E, Zhu Y, Buschhaus JM, et al. Targeting breast cancer stem cell state equilibrium through modulation of redox signaling. Cell Metab 2018;28:69–86.e6.
38. Zhang K, Chen D, Ma K, Wu X, Hao H, Jiang S. NAD(P)H:Quinone oxidoreductase 1 (NQO1) as a therapeutic and diagnostic target in cancer. J Med Chem 2018;61:6983–7003.
39. Starcher CL, Pay SL, Singh N, Yeh I-J, Bhandare SB, Su X, et al. Targeting base excision repair in cancer: NQO1-bioactivatable drugs improve tumor selectivity and reduce treatment toxicity through radiosensitization of human cancer. Front Oncol 2020;10:1575.
40. Huang X, Motea EA, Moore ZR, Yao J, Dong Y, Chakrabarti G, et al. Leveraging an NQO1 bioactivatable drug for tumor-selective use of poly(ADP-ribose) polymerase inhibitors. Cancer Cell 2016;30:940–52.
41. Yang Y, Zhang Y, Wu Q, Cui X, Lin Z, Liu S, et al. Clinical implications of high NQO1 expression in breast cancers. J Exp Clin Cancer Res 2014;33:14.
42. Mikami K, Naito M, Ishiguro T, Yano H, Tomida A, Yamada T, et al. Immunological quantitation of DT-diaphorase in carcinoma cell lines and clinical colon cancers: advanced tumors express greater levels of DT-diaphorase. Jpn J Cancer Res 1998;89:910–5.
43. Cui X, Jin T, Wang X, Jin G, Li Z, Lin L. NAD(P)H:quinone oxidoreductase-1 overexpression predicts poor prognosis in small cell lung cancer. Oncol Rep 2014;32:2589–95.
44. Lin L, Qin Y, Jin T, Liu S, Zhang S, Shen X, et al. Significance of NQO1 overexpression for prognostic evaluation of gastric adenocarcinoma. Exp Mol Pathol 2014;96:200–5.
45. Lin L, Sun J, Tan Y, Li Z, Kong F, Shen Y, et al. Prognostic implication of NQO1 overexpression in hepatocellular carcinoma. Hum Pathol 2017;69:31–7.
46. Ma Y, Kong J, Yan G, Ren X, Jin D, Jin T, et al. NQO1 overexpression is associated with poor prognosis in squamous cell carcinoma of the uterine cervix. BMC Cancer 2014;14:414.
47. Li R, Bianchet MA, Talalay P, Amzel LM. The three-dimensional structure of NAD(P)H:quinone reductase, a flavoprotein involved in cancer chemoprotection and chemotherapy: mechanism of the two-electron reduction. Proc Natl Acad Sci U S A 1995;92:8846–50.
48. Oh E-T, Kim J-W, Kim JM, Kim SJ, Lee J-S, Hong S-S, et al. NQO1 inhibits proteasome-mediated degradation of HIF-1α. Nat Commun 2016;7:13593.
49. Li Z, Zhang Y, Jin T, Men J, Lin Z, Qi P, et al. NQO1 protein expression predicts poor prognosis of non-small cell lung cancers. BMC Cancer 2015;15:207.
50. Parkinson EI, Hergenrother PJ. Deoxynyboquinones as NQO1-activated cancer therapeutics. Acc Chem Res 2015;48:2715–23.

51. Pink JJ, Planchon SM, Tagliarino C, Varnes ME, Siegel D, Boothman DA. NAD(P)H:Quinone oxidoreductase activity is the principal determinant of beta-lapachone cytotoxicity. J Biol Chem 2000;275:5416–24.
52. Gerber DE, Beg MS, Fattah F, Frankel AE, Fatunde O, Arriaga Y, et al. Phase 1 study of ARQ 761, a beta-lapachone analogue that promotes NQO1-mediated programmed cancer cell necrosis. Br J Cancer 2018;119:928–36.
53. Beg MS, Huang X, Silvers MA, Gerber DE, Bolluyt J, Sarode V, et al. Using a novel NQO1 bioactivatable drug, beta-lapachone (ARQ761), to enhance chemotherapeutic effects by metabolic modulation in pancreatic cancer. J Surg Oncol 2017;116:83–8.
54. Motea EA, Huang X, Singh N, Kilgore JA, Williams NS, Xie XJ, et al. NQO1-dependent, tumor-selective radiosensitization of non-small cell lung cancers. Clin Cancer Res 2019;25:2601–9.
55. Li X, Liu Z, Zhang A, Han C, Shen A, Jiang L, et al. NQO1 targeting prodrug triggers innate sensing to overcome checkpoint blockade resistance. Nat Commun 2019;10:3251.
56. Lundberg AP, Boudreau MW, Selting KA, Chatkewitz LE, Samuelson J, Francis JM, et al. Utilizing feline oral squamous cell carcinoma patients to develop NQO1-targeted therapy. Neoplasia 2021;23:811–22.
57. Traver RD, Siegel D, Beall HD, Phillips RM, Gibson NW, Franklin WA, et al. Characterization of a polymorphism in NAD(P)H: quinone oxidoreductase (DT-diaphorase). Br J Cancer 1997;75:69–75.
58. Tsvetkov P, Adamovich Y, Elliott E, Shaul Y. E3 ligase STUB1/CHIP regulates NAD(P)H:quinone oxidoreductase 1 (NQO1) accumulation in aged brain, a process impaired in certain Alzheimer disease patients. J Biol Chem 2011;286:8839–45.
59. Papa L, Hahn M, Marsh EL, Evans BS, Germain D. SOD2 to SOD1 switch in breast cancer. J Biol Chem 2014;289:5412–6.
60. Győrffy B. Survival analysis across the entire transcriptome identifies biomarkers with the highest prognostic power in breast cancer. Comput Struct Biotechnol J 2021;19:4101–9.
61. Madajewski B, Boatman MA, Chakrabarti G, Boothman DA, Bey EA. Depleting tumor-NQO1 potentiates anoikis and inhibits growth of NSCLC. Mol Cancer Res 2016;14:14–25.
62. Bock FJ, Tait SWG. Mitochondria as multifaceted regulators of cell death. Nat Rev Mol Cell Biol 2020;21:85–100.
63. Korshunov SS, Krasnikov BF, Pereverzev MO, Skulachev VP. The antioxidant functions of cytochrome c. FEBS Lett 1999;462:192–8.
64. Pan Q, Kleer CG, van Golen KL, Irani J, Bottema KM, Bias C, et al. Copper deficiency induced by tetrathiomolybdate suppresses tumor growth and angiogenesis. Cancer Res 2002;62:4854–9.
65. Hassouneh B, Islam M, Nagel T, Pan Q, Merajver SD, Teknos TN. Tetrathiomolybdate promotes tumor necrosis and prevents distant metastases by suppressing angiogenesis in head and neck cancer. Mol Cancer Ther 2007;6:1039–45.
66. Lowndes SA, Harris AL. Copper chelation as an antiangiogenic therapy. Oncol Res 2004;14:529–39.
67. Ramchandani D, Berisa M, Tavarez DA, Li Z, Miele M, Bai Y, et al. Copper depletion modulates mitochondrial oxidative phosphorylation to impair triple negative breast cancer metastasis. Nat Commun 2021;12:7311.
68. Lowndes SA, Adams A, Timms A, Fisher N, Smythe J, Watt SM, et al. Phase I study of copper-binding agent ATN-224 in patients with advanced solid tumors. Clin Cancer Res 2008;14:7526–34.
69. Lamb R, Bonuccelli G, Ozsvári B, Peiris-Pagès M, Fiorillo M, Smith DL, et al. Mitochondrial mass, a new metabolic biomarker for stem-like cancer cells: understanding WNT/FGF-driven anabolic signaling. Oncotarget 2015;6:30453–71.